Disentangling the roles of late Miocene palaeogeography and vegetation – implications for climate sensitivity

Catherine D. Bradshaw[a]*, Daniel J. Lunt[a], Rachel Flecker[a], Taraka Davies-Barnard[a]

a Bristol Research Initiative for the Dynamic Global Environment (BRIDGE), School of Geographical Sciences, University of Bristol, University Road, Bristol BS8 1SS, UK

Correspondence to: C.D. Bradshaw (Catherine.Bradshaw@gfi.uib.no; +47 55584787)

Abstract

The impact of rising CO_2 on future climate remains uncertain but the evidence for high CO_2 in the palaeorecord suggests that past climates could provide a potentially quantifiable indication of climate in a high-CO_2 world. One such past time period is the Late Miocene (11.6-5.3 Ma), for which paleo-CO_2 reconstructions indicate higher levels than those of preindustrial, and similar to the present atmospheric level (~ 400ppm). The Late Miocene palaeorecord suggests a much warmer and wetter Northern Hemisphere than preindustrial. However, vegetation feedbacks are an important component of the climate system and vegetation distributions reconstructions from the palaeorecord have been shown to be very different to the present vegetation distribution. We examine the role that different vegetation and palaeogeography plays in climate sensitivity for the late Miocene and consider the implications for potential future climate change. To do this we use coupled atmosphere-ocean-vegetation simulations of late Miocene and potential modern climates forced by three different CO_2 concentrations with vegetation perturbation experiments and make quantitative comparisons to the palaeorecord. Optimal regions to target late Miocene palaeodata acquisition for the purposes of informing about future climate include North America, northern Africa, Australia, Paraguay and southern Brazil, and northeastern Asia. These regions are those which the model results predict to be most sensitive to CO_2 forcing, but where the local temperature response to CO_2 forcing is similar between the simulated potential modern and late Miocene climates. The model results suggest that climate sensitivity to CO_2 forcing is directly affected by the palaeogeographic configuration and that the inferred climate sensitivity for doubled CO_2 is 0.5-0.8°C higher for the late Miocene than we might expect for future climate because of differences in synergy. The greater land mass at high northern latitudes during the late Miocene and the differences in vegetation distribution predictions that result, combined with differences in ocean circulation and the effect of sea ice, make the late Miocene boundary conditions more sensitive to CO_2 forcing than the modern boundary conditions.

Climate modelling; late Miocene; vegetation; CO_2; palaeogeography; climate sensitivity

1 Introduction

Reconstructions of late Miocene (11.6-5.3 Ma) CO_2 range from 144 to 1350ppm but most data suggest CO_2 levels were between preindustrial (280ppm) and modern (400ppm) concentrations (Demicco et al., 2003; Freeman and Hayes, 1992; Kurschner et al., 2008; Kurschner et al., 1996; Pagani et al., 1999a; Pagani et al., 1999b; Pagani et al., 2010; Pearson and Palmer, 2000; Tripati et al., 2011; Zhang et al., 2013; and see Figure 1 of Bradshaw et al., 2012). The palaeorecord also suggests that, for regions with abundant late Miocene data (in southern Europe and in central and southern Asia), the climate was generally hotter and/or wetter than today (Bruch et al., 2007; Eronen et al., 2010; Pound et al., 2012; Pound et al., 2011; Utescher et al., 2011; and see Figures 7 and 11 of Bradshaw et al., 2012). The fact that the late Miocene climate was warmer and wetter than today is consistent with the fact that our modern climate has not yet reached equilibrium with our present atmospheric CO_2 concentration (Stocker et al., 2013), However, there could also be underlying differences in climate sensitivity between these two time periods due to differences in the continental and orographic configuration.

In order to use past warm climates to infer potential future climate change, it is important to establish the dependence of feedbacks (and therefore climate sensitivity) on the background climate state (Rohling et al., 2012). Consistent intercomparisons that separate out understanding of climate dynamics due to CO_2 forcing from other potential contributors such as paleogeography (continental positions, ocean gateways and continental ice extent), and associated feedbacks, are therefore essential. Previous work using extensive model-data comparisons suggests that CO_2 rather than paleogeography was the primary driver of late Miocene warmth (Bradshaw et al., 2012) but did not separate out the effects of vegetation. This study focuses on the role of vegetation in determining late Miocene climate and how palaeogeographic differences might affect the vegetation distribution and the sensitivity to CO_2 forcing. We show that palaeogeography is very important in the determination of temperature because it impacts both sensitivity to CO_2 forcing directly through differences in heat capacity, and indirectly through the distribution of high latitude vegetation and the combination of feedback mechanisms.

2 Description of the Models and Experiment Design

2.1 Description of the climate model HadCM3L and the dynamic vegetation model TRIFFID

The general circulation model (GCM) used in this work is HadCM3L (Cox et al., 2000), the low ocean resolution (2.5° latitude by 3.75° longitude) version of the fully coupled atmosphere-ocean model HadCM3 (Gordon et al., 2000; Pope et al., 2000). The atmosphere component has 19 vertical levels and the ocean component has 20 vertical levels and the model is run without the requirement for flux adjustments. Full details of the GCM and comparison to modern observations are given in Appendix B Section 1.1 of Bradshaw et al. (2012).

The interactive global vegetation model coupled to HadCM3L is the Top-down Representation of Interactive Foliage and Flora Including Dynamics (TRIFFID) model, a full description of which is given in Cox (2001) and Hughes et al. (2004). TRIFFID calculates areal coverage, leaf area index and canopy height for five defined plant functional types (PFTs): broadleaf tree, needleleaf tree, C_3 grass, C_4 grass and shrub, all of which can co-exist within the same model grid box. The vegetation model is competitive and hierarchical based on height, so natural vegetation will tend towards trees, if the conditions are suitable. Each PFT responds differently to climate and CO_2 forcing (e.g. C_3 and C_4 grasses use different photosynthetic pathways), and also impact differently on the physical properties of the land surface (i.e. possessing different aerodynamic roughness lengths and albedo properties). In using the TRIFFID model in a paleo context it is inherently assumed that modern vegetation characteristics are appropriate for the late Miocene and this of course may not be a good assumption. However, allowing vegetation distributions to alter with, and feed back to, the climate is a better test of the dependence of climate sensitivity to vegetation distribution than keeping the vegetation fixed at the modern distribution. More details of the TRIFFID model and comparison to modern observations are given in the Supplementary Information.

2.2 Experimental Design

In this study, simulations have been conducted for late Miocene boundary conditions under different CO_2 concentrations and comparisons are made with potential modern climates for the same CO_2 concentrations. The modern climates are derived using TRIFFID-simulated natural vegetation rather than prescribing the true modern vegetation distribution, in order to exclude anthropogenic land-use changes associated with agriculture and urban areas. The continental positions and orographic boundary conditions for the late Miocene simulations are those from Markwick (2007) and are described in detail in Bradshaw et al. (2012). The boundary conditions for the potential modern simulations are those of the UK Met. Office and also described in Bradshaw et al. (2012). The major differences in the late Miocene boundary conditions as compared to the modern boundary conditions are an open Panama Gateway, a closed Bering Strait, a Barents/Kara Sea landmass, an unrestricted Indonesian Seaway, an unglaciated Greenland and reductions in orography for most of the worlds' highest mountain chains (refer to Figure S1 in the Supplementary Information and also Figure 2 of Bradshaw et al., 2012).

Three potential atmospheric CO_2 concentrations are prescribed: 180ppm, 280ppm and 400ppm, all of which lie within the range of uncertainty of the palaeo-CO_2 reconstructions for the late Miocene (Bradshaw et al., 2012 and references therein; Zhang et al., 2013). All other atmospheric gas concentrations are kept at preindustrial values, and a modern orbit is prescribed.

In addition, vegetation-perturbation experiments were conducted whereby vegetation was fixed at the annual mean equilibrium distribution for each alternative CO_2 concentration, allowing the separation of the contribution made to climate from CO_2 forcing and the contribution made from vegetation feedbacks. The experimental design of the model simulations is shown schematically in Figure 1. The GCM was initially run with CO_2 levels set at preindustrial (280ppm) and the TRIFFID model turned on until the model had reached an equilibrium state (~1000 years), then the two additional CO_2 concentration scenarios were spun-off from each of the control simulations and all six simulations continued for a further 1000 years. The TRIFFID model was turned off and the vegetation fixed at the suggested near-equilibrium distributions and the simulations continued for a further 550 years. In addition, the GCM was run with the vegetation distribution fixed for that predicted with a higher or lower CO_2 concentration than the level prescribed in the simulations, e.g. the vegetation distribution in the 400ppm CO_2 scenario is prescribed with the predicted vegetation distribution for the 280ppm equilibrium climate scenario. These additional vegetation-perturbed scenarios were also run for a further 550 years.

The analysis in this paper is carried out using the climatological means of the last 50 years of each simulation. Analysis is performed from the viewpoint of an increase in CO_2, with focus given to the results from increasing CO_2 from 280 to 400ppm, as this is most relevant for immediate future climate. The change from 180ppm to 280ppm represents a radiative forcing of 2.36 W/m^2 and the change from 280ppm to 400ppm represents a radiative forcing of 1.91 W/m^2.

One of the uncertainties in the late Miocene configuration is the 10 soils parameters including soil moisture criteria, thermal capacities and albedo. For this work, globally homogenous values derived from average modern soils are used for the Miocene simulations (refer to Table S2 and Figure S2 in the Supplementary Information). An additional sensitivity experiment was performed whereby the same globally homogenous average values were used with the modern boundary conditions in order to identify the magnitude of this uncertainty on the results presented. An example of the implication of using these homogenous parameters is shown in Figure S2 in the Supplementary Information.

A spreadsheet containing the model output temperature, precipitation and vegetation distribution for the 280 to 400ppm CO_2 increase are provided as Supplementary Information to this manuscript. The BRIDGE resources webpage provides access to further climate variables and the other simulations from this manuscript that may be of interest (http://www.bridge.bris.ac.uk/resources/simulations); click on "Access simulations".

3 Results and Discussion

3.1 Response to CO_2 forcing including vegetation feedbacks

The model results suggest that as CO_2 increases, climate will warm regardless of whether late Miocene or modern boundary conditions are used, with the greatest warming expressed at the high latitudes and in particular over the oceans during their respective winter months as shown in Figure 2, panels A-D. In addition to Northern Hemisphere wintertime (DJF) warming, the mid to high northern latitudes also warm considerably during the summer months (Figure 2, panels A and C).

When comparing the late Miocene to the modern, the regions that differ most in their temperature response to CO_2 forcing are typically those that have undergone the most significant change in geography. The high latitude regions that have changed between land

and ocean (as shown in Figure 2, panels E and F), e.g. the Bering Strait, the Barents/Kara Sea landmass and the Hudson Bay region, all have a significantly different response to CO_2 forcing. One notable exception to this is the North Atlantic which is more sensitive to CO_2 forcing during DJF with late Miocene boundary conditions than with modern boundary conditions. Reasons for these differences in sensitivity to CO_2 forcing are discussed later in Section 4.3.

Spatially, the distribution of precipitation response to increasing CO_2 is similar between the late Miocene boundary conditions and the modern boundary conditions. Both show an increase in precipitation at the high latitudes, particularly during their respective winter months, year-round decreases in precipitation occur over the Amazon and southern Africa and there is an increase in seasonality in Europe; summers becoming drier and winters wetter (Figure 2, panels G-J). However, whilst the magnitude of the high latitude response is similar for the two boundary conditions, the magnitude of the low latitude response is greater for the late Miocene boundary conditions than the modern (Figure 2, panels K-L). There is also a difference in the sign of the response over Indonesia, in both seasons, for the two boundary conditions: increasing CO_2 with late Miocene boundary conditions leads to a decrease in precipitation in this region; increasing CO_2 with modern boundary conditions leads to an increase in precipitation.

3.2 Predicted vegetation distributions

3.2.1 Vegetation response to CO_2 forcing

Although the broad changes in vegetation distribution as a result of CO_2 forcing are similar for the two sets of boundary conditions, there are some notable differences. The response of trees to CO_2 forcing is similar under both the late Miocene and modern boundary conditions, experiencing a global poleward shift in distribution from 180 to 280ppm and from 280 to 400ppm (Figure 3, panels A-C and Figure 4, panels A-C). Vegetation changes made by the TRIFFID model occur based on climatic thresholds for photosynthesis (temperature and atmospheric CO_2) and a competition hierarchy (trees-shrubs-grasses), refer to Section S1 in the Supplementary Information for more details. As increasing CO_2 inherently leads to an increase in the rate of photosynthesis directly through stomatal conductance (Ainsworth and Rogers, 2007; Farquhar and Sharkey, 1982) and indirectly through temperature increases from the greenhouse gas effect (Berry and Downton, 1982), it is expected that increasing CO_2 will lead to an increase in vegetation cover provided that water is not a limiting factor. Therefore, since trees are at the top of the PFT hierarchy, any increase in temperatures or atmospheric CO_2 will lead to an increase in tree coverage if the other climatic conditions permit. Warmer temperatures directly increase the rate of photosynthesis, and the temperature thresholds that determine photosynthesis are exceeded for longer durations throughout the year leading to an increase in net primary productivity. As precipitation increases with CO_2 forcing in the higher latitudes during the winter months, the soil is able to store moisture in the deeper layers that the trees are able to access during the summer months, thereby countering the reduction in precipitation that occurs across the 40-60°N latitude band during this season when photosynthesis is at a maximum.

This poleward shift is consistent with other studies of the response of vegetation to CO_2 forcing under modern boundary conditions (e.g. Alo and Wang, 2008; Cramer et al., 2001; Emanuel et al., 1985; Gerber et al., 2004; Joos et al., 2001; Scholze et al., 2006; Solomon, 1986) and there is also some observational evidence which may support this response

(Bogaert et al., 2002; D'Arrigo et al., 1987; Lucht et al., 2002; Myneni et al., 1997). Also consistent with this poleward shift are palaeo-biome reconstructions that place both boreal and temperate forest at higher northern latitudes in the late Miocene than is seen today (Pound et al., 2012; Pound et al., 2011).

3.2.2 Regional details

An exception to the poleward shift in tree distribution is in the southern part of Africa. As CO_2 increases from 180ppm to 280ppm, an increase in tree cover is seen for both sets of boundary conditions. Accompanying the increase in tree coverage is a decrease in soil moisture in the tree rooting zone of 80kg/m^2 for the late Miocene boundary conditions and more than 250kg/m^2 for the modern boundary conditions. Analysis of the soil sensitivity experiments shows that this difference is as a result of the differences in the specified soil parameters with the modern homogenous soil results extremely similar to the late Miocene results. However, as CO_2 increases further from 280ppm to 400ppm, there is a decrease in tree cover for both sets of boundary conditions. Soil moisture availability in the tree rooting zone is further depleted by 100kg/m^2 for the late Miocene boundary conditions and by 70kg/m^2 for the modern boundary conditions – for the modern boundary conditions this puts available soil moisture in this region down to around 150kg/m^2. The soil moisture availability combined with a reduction in wintertime precipitation means that water reserves are not replenished to cover the summertime and so water becomes a limiting factor and the trees cannot compete. Vegetation under this higher CO_2 transition in this part of Africa therefore returns to more of a mix of shrubs and bare soil, although trees remain the dominant vegetation type.

The Amazon Rainforest also shrinks under both sets of boundary conditions as CO_2 increases, but a 2% greater reduction occurs for the late Miocene boundary conditions than the modern boundary conditions. Reductions in the size of the Amazon Rainforest are important both in terms of capacity as a major carbon sink and in terms of regional feedbacks to climate (Cox et al., 2000). The reduction of tropical forest with increasing CO_2 was found to be a robust feature of vegetation response across the IPCC AR4 scenarios (Alo and Wang, 2008; Salazar et al., 2007; Scholze et al., 2006), although the HadCM3 model resulted in the greatest response of the Amazon Rainforest (Alo and Wang, 2008).

Shrub coverage also shifts poleward in the Northern Hemisphere as CO_2 increases from 180ppm to 280ppm (Figure 3, panels G and I and Figure 4, panel G and I) but when CO_2 increases from 280ppm to 400ppm an additional northward advance is seen under late Miocene boundary conditions that is does not occur to the same degree under modern boundary conditions (Figure 3, panel H compared to Figure 4, panel H) because the shrubs have already colonised the most northerly grid boxes available to them in the lower 280ppm simulation (i.e. the late Miocene configuration allows for further northward expansion into ice-free Greenland and into the Barents/Kara Sea landmasses).

As with the shrubs, grasses also shift poleward in the Northern Hemisphere for late Miocene boundary conditions as CO_2 increases from 180 to 280ppm (Figure 3, panel D and F), but, apart from a few isolated grid boxes in Greenland and the Canadian Archipelago, no northward shift is seen under modern boundary conditions (Figure 4, panel D and F). When the CO_2 increases further, from 280 to 400ppm, an equatorward shift in grass distribution results for both sets of boundary conditions but particularly for late Miocene boundary conditions (Figure 3, panel E compared to Figure 4, panel E). The magnitude of global grass coverage reduces with increasing CO_2 for both sets of boundary conditions. An 11% reduction in area occurs as CO_2 increases from 180ppm to 280ppm and a further 8% reduction in area arises as CO_2 increases from 280 to 400ppm under late Miocene boundary conditions. For the modern boundary conditions, the equivalent figures are a 12% reduction as CO_2 increases from 180ppm to 280ppm and a further 5% reduction as CO_2 increases from 280 to 400ppm. Changes to the distribution of bare soil are small for both sets of boundary conditions (Figure 3, panels J-L and Figure 4, panels J-L).

3.2.3 Dominant vegetation types

Figure 5 shows the evolution of global vegetation as CO_2 increases. At the global scale, when the CO_2 concentration is 180ppm the dominant vegetation type for the late Miocene boundary conditions is grasses (40% of the total vegetated land area) whereas for the modern boundary conditions grasses and trees are approximately equal in areal coverage (32% for grasses, 31% for trees). At 280ppm the dominant vegetation type for both sets of boundary conditions changes to trees and this remains the dominant vegetation type as CO_2 increases to 400ppm. Shrubs increase in areal coverage between 180 and 280ppm but then decrease between 280 and 400ppm for both sets of boundary conditions. The extent of bare soil (i.e. desert) as the dominant surface cover remains constant at around 20% of the total land area available for vegetation for both the late Miocene and the modern boundary conditions. Although the poleward shift in tree cover was greatest for the late Miocene boundary conditions as described in Section 3.2.1, there is a greater magnitude of tree coverage in the Southern Hemisphere, in South America in particular, with the modern boundary conditions and therefore at the global scale the modern boundary conditions yield the greatest areal coverage of trees. Regional differences are now discussed in more detail.

The dominant vegetation predicted under each CO_2 scenario clearly reveals the poleward advance of latitudinal bands of grasses, shrubs and trees in the Northern Hemisphere. As the late Miocene configuration has more land available for vegetation at high northern latitudes than the modern configuration (ice-free Greenland, a closed Bering Strait, the Barents/Kara Sea landmasses, a closed Hudson Bay), the latitudinal bands advance farther northwards than with the modern boundary conditions (Figure 6, panels A-C compared to D-F).

For the 180ppm and 280ppm CO_2 levels, the bare soils that dominate the potential modern boundary conditions around Greenland and the Canadian Archipelago are dominated by grasses in the late Miocene (Figure 6, panels A-B compared to D-E). For the increase in CO_2 from 280 to 400ppm, the grasses that dominated the high northern latitudes at the lower CO_2 concentrations are replaced by shrubs and trees suggesting enhanced warming (Figure 6, panels C and F). For all of the CO_2 concentrations, central Asian deserts extend further north in the potential modern simulation as compared to the late Miocene simulation and the southwestern North American deserts do not feature in the Miocene. Conversely, the open Panama Gateway in the late Miocene is surrounded by deserts whereas forests dominate in those equivalent grid boxes surrounding Central America for the potential modern.

In the Southern Hemisphere, the principle differences between the late Miocene and the modern simulations are found in the Amazon Rainforest, which turns to grassland and desert for both boundary conditions, but has a greater extent of desert for the late Miocene. In Australia, the late Miocene simulations predict more grass cover than the potential modern simulations, although the vegetation predicted by TRIFFID for Australia with modern boundary conditions is perhaps questionable given the lack of desert simulated (Figure 6, panels E and F).

Soil sensitivity experiments show only minor differences in vegetation predictions resulting from the homogenous soils parameters as compared to the true soils parameters (see discussion and Figure S3 in the Supplementary Information).

Analysis

3.3 Separation of CO_2 forcing and vegetation feedbacks

The vegetation and CO_2 feedbacks can combine non-linearly; therefore it is useful to disassociate them in order to consider their impacts separately. To evaluate the role of CO_2 forcing in determining climate the simulations that keep vegetation fixed but alter CO_2 are compared. To evaluate the role of vegetation changes in determining climate the simulations that keep CO_2 fixed but alter the vegetation distributions are compared. The factor separation technique of Lunt et al. (2012) is used to assess the two contributions of CO_2 forcing and vegetation as follows:

$$f_{CO2} = \frac{1}{2}\left((\mathrm{C400V280} - \mathrm{C280}_{\mathrm{TRIF}}) + (\mathrm{C400}_{\mathrm{TRIF}} - \mathrm{C280V400})\right) \qquad (1)$$

$$f_{VEG} = \frac{1}{2}\left((\mathrm{C280V400} - \mathrm{C280}_{\mathrm{TRIF}}) + (\mathrm{C400}_{\mathrm{TRIF}} - \mathrm{C400V280})\right) \qquad (2)$$

where, f_{CO2} is the contribution from CO_2 forcing and f_{VEG} is the contribution from the vegetation changes.

The contribution to the temperature increase from CO_2 forcing alone occurs with a similar distribution to that described for CO_2 forcing with vegetation changes, suggesting that the CO_2 forcing dominates (Figure 7 compared to Figure 2). The greatest warming occurs at high latitudes during winter months with the largest increases over the oceans (Figure 7, panels A-B and E-F).

CO_2 forcing alone cannot account for all of the warming; the temperature increases are lower than those predicted with vegetation changes included. Figure 7, panels A-D shows the CO_2 contribution as a result of increasing from 280 to 400ppm, but the results for increasing from 180 to 280ppm are very similar. Globally, the contribution of direct CO_2 forcing accounts for 2.5°C of the annual temperature increase when CO_2 increases from 180ppm to 280ppm but this reduces to 1.9°C of the annual temperature change when CO_2 is increased from 280 to 400ppm.

The distribution of precipitation changes as a result of increasing CO_2 only (Figure 7, panels C-D and G-H) is also extremely similar to that with the vegetation changes included.

The contribution to the overall warming that can be assigned to vegetation changes is 1-2°C less globally averaged than that contributed by the CO_2 forcing alone (1.5-2.5°C), but it is by no means insignificant regionally with up to 2.5°C of warming across the mid-high northern latitudes and 4°C for some parts of the north Pacific Ocean for the 280 to 400ppm CO_2 vegetation distribution change (Figure 7, panels I-J and M-N). For the simulations which alter the vegetation distribution but keep CO_2 fixed (C280V280-C280V180 and C400V400-C400V280), the surface albedo changes are associated with the warming seen, for both sets of boundary conditions. For the 180ppm to 280ppm vegetation change, reductions in albedo of up to 20% result in JJA across the mid-high northern latitudes and reductions of up to 40% occur in DJF between 40 and 60°N in North America and Western Europe. The snow cover north of 60°N increases by up to 10% for this vegetation change, consistent with the increase in winter precipitation. The vegetation changes between 280 and 400ppm yield a similar magnitude of surface albedo reduction but this extends over a greater spatial area (40-80°N) and a greater temporal domain (DJF through to MAM), and reductions of up to 20% are also seen in SON and 10% in JJA. The albedo change can be explained by changes in the albedo of the vegetation itself. In the model, shrubs and grasses are assigned a snow-free albedo of 20% compared to trees at 10%, and a 40-60% albedo when snow covered compared to just 15% for trees. Reductions in snow cover, which give even larger albedo changes, are also responsible. For the 280 to 400ppm vegetation change, in DJF snow cover reduces by up to 20% across the 50-60°N latitudinal band and by 40% across the 40-50°N latitudinal band. Reductions of up to 30% are also seen in MAM and SON between 40 and 70°N, and above 70°N the reductions are 10-20%. Due to the greater extent of land at the high northern latitudes under the late Miocene boundary conditions (Greenland, closed Bering Strait, Barents/Kara Sea landmass), the albedo reductions are greater than occurs with the modern boundary conditions. The DJF albedo changes are expressed most strongly in the oceans rather than on land because of the sensitivity of sea ice to temperature fluctuations.

Our results contrast with that from other work investigating of the impact of late Miocene vegetation on climate by Knorr et al. (2011), where the warming contributed by the Northern Hemisphere-dominated vegetation changes was translated to the Southern Hemisphere. For the Northern Hemisphere summer months, the warming that the late Miocene boundary conditions yield is widespread but Southern Hemisphere temperature changes are mostly not significant (Figure 7, panels I-J). The average temperature increase in the Southern Hemisphere as a result of vegetation changes is just 0.1°C. Given the limited vegetation-covered land area and the smaller magnitude of the vegetation distribution changes in the

Southern Hemisphere as compared to the Northern Hemisphere, it is not surprising that the greatest warming from vegetation feedbacks occurs in the Northern Hemisphere. However, it is notable that the vegetation feedbacks from the Northern Hemisphere are not translated to the Southern Hemisphere for the late Miocene boundary conditions but are for the modern boundary conditions (Figure 7, panels M and N compared to I and J). This is because in all of the late Miocene simulations North Atlantic overturning has virtually shut down completely (<2Sv at 180ppm, <1Sv at 280ppm and 400ppm). The different late Miocene results may be due to model or boundary condition differences, as the Knorr et al. (2011) model simulations maintain a North Atlantic overturning circulation. The extent of North Atlantic overturning during the late Miocene remains controversial with some records indicating strong North Atlantic Deep Water (NADW) production during the late Miocene (Blanc et al., 1980; Delaney, 1990; Keller and Barron, 1983; Miller and Fairbanks, 1985; Woodruff and Savin, 1989; Wright et al., 1992) whilst others indicate a significant increase in the early Pliocene implying weaker production during the Miocene (Billups et al., 1999; Haug and Tiedemann, 1998; Tiedemann and Franz, 1997), consequently we are unable to discount either model result. Modelling studies have also demonstrated a significant impact of vegetation on overturning circulation through changes in the hydrological cycle (Ganopolski et al., 1998; Zhou et al., 2012). Therefore, should a stronger North Atlantic overturning be appropriate for the late Miocene than is seen with the model used here, such impacts may alter the results presented: surface salinity increases in the North Atlantic by up to 1PSU year-round when the vegetation is changed from a 280ppm to a 400ppm distribution, and sea surface temperatures in the same location decrease by up to 2°C suggesting that strengthening of an active North Atlantic overturning circulation would result.

Changes to the hydrological cycle as a result of the vegetation changes imposed also explain some of the resultant warming, particularly in the tropics. For example, in the Amazon the vegetation changes imposed reflect a desertification process, whereby trees are lost around the periphery of the rainforest and replaced with shrubs and grasses as CO_2 increases from 180 to 280ppm. As CO_2 increases further to 400ppm, those shrubs and grasses are themselves replaced by bare soil, the periphery of the remaining forest loses trees and the size of the overall deforestation/desertification expands. Both stages of the vegetation change result in evapotranspiration reductions of up to 1.5mm/day and associated reductions in latent heat of up to 45W/m^2 with the late Miocene boundary conditions. Associated with this change in energy flux are increases in sensible heat of up to 17W/m^2 causing near surface temperature to increase (Seneviratne et al., 2010); temperature increases over the Amazon are up to 3.1°C. It should be noted however, that the Amazon Rainforest simulated by HadCM3L under a modern preindustrial climate covers slightly too large an area and the northeastern Amazon is simulated to be dominated by grasses rather than trees.

In contrast, over India the vegetation changes are mainly afforestation – bare soil is replaced with grasses, shrubs and trees as CO_2 increases from 180 to 280ppm and evapotranspiration rates and latent heat flux increases accordingly by up to 0.8mm/day and 24W/m^2 respectively with the late Miocene boundary conditions. However, increases in sensible heat (up to 17W/m^2) only occur during DJF when temperature increases of up to 3.8°C are seen. Some of the temperature change in DJF may therefore be related to changes in the hydrologic cycle, but albedo reductions of up to 20% also occur in this season as a result of both direct vegetation changes and reductions in snow cover itself (up to 30% in the Himalayas). In JJA sensible heat decreases by 9.5W/m^2 and so temperature actually decreases here by 1.4°C during the monsoon season due to changes in the hydrologic cycle, countering the JJA albedo reduction of 5% that would otherwise result in warming. However, for most of the grid boxes in this region, the temperature decrease is not significant at the 95% confidence level.

Precipitation reduces in JJA over the Amazon Rainforest by 40-50% in response to CO_2-induced vegetation distribution changes (Figure 7, panels K and O). A northward shift of the ITCZ is seen consistent with studies of afforestation in the Northern Hemisphere (e.g. Swann et al., 2012), though the magnitude of change is less than that resulting from the CO_2 increase itself. Many studies, model-based and observational, also link soil moisture and evapotranspiration to precipitation, although the processes involved are complex (Carson and Sangster, 1981; Dirmeyer and Shukla, 1994; Eltahir, 1998; Findell and Eltahir, 1997; Levis et al., 2004; Mintz, 1984; Oglesby and Erickson III, 1989). Over the Amazon region, both reductions in soil moisture and precipitation result from the vegetation changes, and Asian monsoon precipitation doubles for the late Miocene boundary conditions, consistent with these studies.

3.4 Synergy

Individual contributions to complex processes such as climate dynamics may not add linearly and the extent of that non-linearity is termed the synergy. We use the factor separation technique of Lunt et al. (2012) to assess synergy between the two contributions of CO_2 forcing and vegetation as follows:

$$f_{SYN} = C400_{\mathrm{TRIF}} - C280V400 - C400V280 + C280_{\mathrm{TRIF}} \quad (3)$$

where, f_{SYN} is the synergy term defined as going from the lower CO_2 to the higher CO_2. Table 1 presents the factor separation (Equations 1 and 2) and the synergy term calculations.

Synergy is a measure of the non-linearity of the combination of individual contributions from CO_2 forcing and vegetation changes, and in some regions quite significant synergy is seen. Mostly the warming contributed by the CO_2 increase and the warming contributed by the vegetation changes sum to greater than the warming seen with both mechanisms included simultaneously (Figure 8, panels A-D). In other words, globally, the synergy for temperature between direct CO_2 forcing and vegetation changes is negative annually for the late Miocene boundary conditions, -0.2°C (180ppm to 280ppm) and -0.1°C (280ppm to 400ppm). For the modern boundaries conditions, the negative synergy is of a greater magnitude, -0.3°C (180ppm to 280ppm) and -0.5°C (280ppm to 400ppm).

For precipitation, the pattern of synergy is more complex (Figure 8, panels E-H). The synergy in annual precipitation at the global scale is also negative at -3.3mm/year (180ppm to 280ppm) and -0.9mm/year (280ppm to 400ppm) for late Miocene boundary conditions, and -4.0mm/year (180ppm to 280ppm) and -3.4mm/year (280ppm to 400ppm) for modern boundary conditions (Table 1).

3.5 Climate Sensitivity

The global mean annual 1.5m air temperatures from the simulations have a slightly non-linear relationship with the CO_2 concentration (refer to Figure 9). The difference between the late Miocene and the potential modern climates is small at 180ppm: the modern climate is 0.05°C warmer and 1.5mm/year wetter annually than the late Miocene at the global scale. However, between 180 and 280ppm CO_2 the late Miocene climate becomes warmer and wetter than the modern climates and the gap between the two widens as CO_2 increases further to 400ppm. At 400ppm, the late Miocene boundary conditions are 0.6°C warmer and 7mm/year wetter than the modern boundary conditions. The late Miocene boundary conditions result in a 0.5°C higher climate sensitivity overall than modern boundary conditions, with little difference occurring whether the CO_2 increase is from the lower baseline of 180ppm or the preindustrial level of 280ppm (Table 2). However, both the modern and the late Miocene sensitivities are high in relation to the estimates from the CMIP5 models (Stocker et al., 2013), but slightly lower than recent estimates for the Eocene using the same model (Loptson et al., 2014).

Vegetation changes can alter moisture fluxes and therefore the local hydrological cycle and temperatures. The vegetation changes simulated here make a significant change to the overall sensitivity to CO_2 forcing of the late Miocene simulations, increasing climate sensitivity by 1.2°C when the CO_2 increase is from a baseline of 180ppm and 1.4°C when the CO_2 increase is from a baseline of 280ppm (refer to Table 3). The vegetation changes under the modern boundary conditions contribute much less to the overall climate sensitivity, particularly when the CO_2 increase is from 280ppm to 400ppm (only 0.4°C; Table 3), due to differences in synergy as discussed in Section 3.4.

The different late Miocene boundary conditions and vegetation distributions make the temperature response to CO_2 forcing more sensitive overall than the modern geography and potential modern vegetation distributions do. We attribute this difference to several processes. Firstly, as the late Miocene simulations are warmer than the equivalent modern simulations there is a greater sea ice loss in the late Miocene simulations than the equivalent modern simulations for the same CO_2 change globally and therefore the positive sea ice feedback mechanism is strongest with the late Miocene boundary conditions (Figure 10). In the North Atlantic, although more sea ice is lost in the late Miocene simulations than the modern simulations, the initial extent of sea ice is much greater under the late Miocene boundary conditions and therefore the surface albedo remains high in this region despite the CO_2 increases. In the North Atlantic, the shutdown of North Atlantic Deep Water (NADW) production and the associated overturning in the Atlantic for the late Miocene leads to a reduced poleward heat transport in the Northern Hemisphere as compared to the modern simulations and the greater sea ice extent in the North Atlantic for the late Miocene, consistent with studies of reductions in NADW production (e.g. Álvarez-Solas et al., 2011). However, we suggest that the high albedo deriving from the extensive sea ice is offset in the late Miocene simulations by the albedo reductions deriving from the changes made to the Greenland Ice Sheet and the Barents/Kara Sea landmass. The Greenland Ice Sheet is much reduced in the late Miocene and Greenland is dominated by the shrub PFT at 400ppm (refer to Figure 6, panel C), therefore although the majority of Greenland is snow-covered in winter, the albedo is 20% lower than in the modern simulations. Likewise, the Barents/Kara Sea landmass, covered by shrubs and trees in the late Miocene, has a lower albedo than the equivalent ocean grid boxes in the modern simulations which are covered by sea ice. The change in sensitivity can vary seasonally. For example, the Hudson Bay and Barents/Kara Sea regions, as land in the late Miocene but ocean today, are more sensitive to CO_2 forcing in JJA but less sensitive in DJF (Figure 2, panels E and F). In JJA, this is because the ocean has a higher specific heat capacity than the land surface and so this region will warm faster in the late Miocene as land than it does today as ocean, and additionally, the input of cold water due to sea ice melt will constrain the modern surface waters to near freezing point whereas in the late Miocene no such constraint exists. This region also exhibits 20% less low cloud cover in the late Miocene simulations than in the modern simulations during JJA indicating a role for cloud feedbacks in modulating the modern climate more than the late Miocene climate in this season. In DJF, the modern ocean covered by sea ice is more sensitive to CO_2-induced warming because of the sea ice-albedo feedback mechanism and changes to the insulation that sea-ice provides between the atmosphere and the underlying warmer ocean.

The second mechanism we suggest leads to the differences between the two boundary conditions is ocean ventilation. As NADW production is very weak in the late Miocene simulations, Antarctic Bottom Water production is the primary driver of ocean ventilation under those conditions. The strength of the resultant overturning in the South Atlantic is ~ 8Sv stronger in the late Miocene simulations than the modern simulations and so strong southern-focussed ocean ventilation keeps the Southern Hemisphere warmer in the late Miocene simulations than in the modern simulations (at 280ppm CO_2, the late Miocene Southern Hemisphere is 1.4°C warmer than the modern Southern Hemisphere). As strong North Atlantic overturning circulation exerts a relative cooling influence on the Southern Hemisphere, this is a negative feedback mechanism for the simulations with modern boundary conditions. Increasing CO_2 acts to dampen overturning in the North Atlantic under both sets of boundary conditions, but amplifies the overturning in the Southern Ocean by 1Sv more under late Miocene boundary conditions than under modern boundary conditions. This increase in southern-focussed overturning, and therefore enhancement of equator-to-pole heat distribution in the Southern Hemisphere, explains the warming seen on Antarctica (Figure 7, panel A compared to E and B compared to F) under late Miocene boundary conditions compared to modern boundary conditions.

However, the soil parameters also affect the sensitivity to CO_2 forcing – changing the soils parameters from homogenous values to the true modern soils parameters reduces climate sensitivity under modern boundary conditions by up to 0.25°C (refer to Table 2). When globally homogenous soil parameters are used in the modern simulations the climate becomes globally cooler and drier (refer to Figure 9) and we can hypothesise that the late Miocene climate would respond in the same way: if late Miocene soils were similar to modern then the results documented here represent a minimum (i.e. that the climate would get warmer and wetter and the absolute difference between the late Miocene climate and the potential modern climate would increase), but late Miocene soils sensitivity experiments are needed for confirmation, e.g. setting the late Miocene soils to be the same as modern soils. In addition, many soil properties such as the albedo, soil water storage capacity and soil texture, which remain constant throughout the simulations presented here, would actually vary through time as climate and vegetation change both seasonally and on longer timescales,. A recent study using a model capable of altering these properties throughout the model integration (Stärz et al., 2013) found that the soil changes amplified the climate signal in both warmer (Holocene) and cooler (LGM) conditions and so this could be an important feedback mechanism missing from the work presented here.

3.6 Model-Data Comparison

We compare the late Miocene experiments with the available late Miocene proxy data to help establish whether our model can reproduce late Miocene conditions and perhaps constrain the uncertainty in the palaeo-CO_2 record. Comparisons are made with the palaeorecord using the quantitative terrestrial reconstructions and model-data comparison methodology detailed in Bradshaw et al. (2012). This methodology assumes that whilst the model-derived temperatures and precipitations are not necessarily accurate, the relationship between the modern climate and the late Miocene climate is robust and bias corrections using the offset between modern observations and the simulated preindustrial climate (280ppm) are applied to the late Miocene climatologies. The results for the model-data comparison are all provided as Figures S6 to S17 of the Supplementary Information of this paper and detailed in Tables S3-6. The results detailed in this section are for the mean annual temperature and the mean annual precipitation. Additional results for the cold month mean temperature and the warm month mean temperature are provided in the Supplementary Information in Section S3.2 and Figure S4. For the late Miocene simulations, a modern orbit has been prescribed, yet the data from the palaeorecord could record the climate from any of the late Miocene orbits. Future work should include comparing these data to different late Miocene orbital configurations to assess the impact of the modern orbit assumed in the work presented here.

Note that we would not expect the results of these fixed vegetation simulations to be completely identical to the simulations described in Bradshaw et al. (2012) because the interactive vegetation model alters the vegetation throughout the year whereas in this work the vegetation is held constant at mean annual fractional coverage and leaf area index, and small differences in the simulated climates are found.

3.6.1 Mean Annual Temperature (MAT)

For the mean annual temperature comparison, it is clear that changing the vegetation and/or the CO_2 concentration has not always resulted in an improvement in the model-data comparison (Figure 11, panel A-D).

North of 45°N for all but 4 sites in Russia the biome reconstructions are forest (Pound et al., 2011) suggesting that the 400ppm vegetation distribution here is accurate. However, for North America, this suggests that either the level of CO_2 was lower than 400ppm, or that the model result is inaccurate for this location because when the vegetation prescribed is that of the 400ppm distribution the simulations with CO_2 set to both 180ppm and 280ppm perform better in this region than the simulation with CO_2 set to 400ppm (refer to Figure 11, panel C compared to D, and Figure 12, panel C). A Pliocene study using the same GCM as employed in this work has found that small amounts of uplift in the North American Cordillera cause significant cooling in this region (Foster et al., 2010). Late Miocene sensitivity studies of the height of the North American Cordillera and also the configuration of the Bering Strait are therefore recommended as future work.

The fact that south of ~ 35°N changing the vegetation and/or the CO_2 concentration makes the model-data comparison deteriorate (Figure 11, panels A-D) suggests that not translating Northern Hemisphere-derived warming to the south through ocean circulation is indeed appropriate for the late Miocene, since the warming that has occurred directly from the vegetation changes here alone makes the simulated MATs too warm as compared to the proxy reconstructions. However, the scarcity in the MAT data for South America, Africa and Australia make drawing any firm conclusions about the temperatures in these regions unwise.

For Europe and central Asia, where most of the late Miocene MAT data is located, there is a clear indication that the vegetation and the CO_2 changes imposed improve the model-data comparison (Figure 11, panels A-D). Regardless of the vegetation distribution imposed, the best-fit CO_2 scenario in this region is 400ppm; the datapoints for which a 180ppm and/or 280ppm CO_2 concentration provide a better fit are located in Spain and around the Mediterranean coastline (Figure 12, panels A-C). A similar pattern arises if the best-fit vegetation distribution is considered – if the CO_2 concentration for the late Miocene was between 280 and 400ppm, away from the Mediterranean coast, the best-fit vegetation is predominantly the 400ppm distribution (Figure 12, panels G-I).

In South-east Asia, only the 180ppm CO_2 concentration scenarios have notable MAT overlap with the data (Supplementary Figure S6). The vegetation changes predicted by the TRIFFID model as CO_2 rises were to increase tree cover and for all of the CO_2 scenarios the dominant PFT in this region is trees; this is in agreement with the biome reconstructions of temperate forest (Pound et al., 2011). Afforestation has been found to have a cooling effect in the tropics (Bonan, 2008) and therefore it might be expected that the vegetation changes imposed should cool the climate, but for this part of South-east Asia this is not the case. It may be that the different palaeogeography of the late Miocene causes this region to respond differently to afforestation than modern studies have found and it may be that the model simulations produce MATs that are too warm as compared to the data because of inaccuracies in the local palaeogeography. A study incorporating two uplift scenarios for the late Miocene using the same model as used in this study (Lunt et al., 2010) simulates total Himalayan uplift (4500m higher, their Emod-Eflat) contributing widespread cooling of at least 4°C in this part of South-east Asia (east of the Himalayas themselves, which cool much more) and both partial uplift configurations (1500m higher, their Efrac-Eflat and 4500m higher but for the southern margins only, their ESouth-Eflat) contributing at least 2°C of cooling in this region, with some parts becoming up to 4°C colder. It could also be that the configuration of the Indonesian Seaway is incorrect for this time period. Further model sensitivity studies are required to investigate these uncertainties on the model-data comparison results.

3.6.2 Mean Annual Precipitation (MAP)

Most of the modelled MAPs overlap with the Messinian precipitation reconstructions (>91%; Table S4), except for a small pocket in the Eastern Mediterranean and in Spain (refer to Supplementary Figures S4 panel 2A and C, panel 2; Figures S9-11, panels A-C). Therefore, the improvements or deteriorations between the model scenarios is small (Figure 11, panels E-H). For the Tortonian however, there are many datapoints which are wetter than the model simulates, located across Europe and into central Asia (Supplementary Figures S4, panel 2B and D; Figures S9-11, panels D-F). In Europe, the sensitivity of precipitation to CO_2 forcing is not even across the region. There is a clear north-south divide in the best-fit CO_2 scenario which is consistent for all of the vegetation distributions, with the north best matching the higher CO_2 scenario and the south the lower CO_2 scenario (Figure 12, panels D-F), and there is a clear east-west divide in the best-fit vegetation scenario which is consistent across all of the CO_2 concentrations, with the east best matching the lower CO_2 vegetation distribution and the west the medium and high CO_2 vegetation distributions (Figure 12, panels J-L). The Tortonian biome reconstructions for Europe are predominantly temperate forest but for all of the CO_2 scenarios the dominant PFT on the Eastern side of Europe is shrubs and for Spain shrubs and bare soil. This suggests that perhaps the Tortonian model-data mismatches in this region could be due to wrongly imposed vegetation. The biome reconstructions for Spain change from temperate forest to xerophytic shrublands between the Tortonian and the Messinian (Pound et al., 2012), which could explain the better fit here with the Messinian precipitation reconstructions.

There are increases in the overall number of model-data overlaps as either CO_2 increases and/or the vegetation prescribed moves to the higher CO_2 distributions, but 33% of the datapoints are still in disagreement with the model simulations.

3.6.3 Targeting palaeodata acquisition

For the purposes of improving our evaluation of the ability of HadCM3L-TRIFFID to reproduce late Miocene climate, quantitative data from the whole Southern Hemisphere and

North America is lacking. However, for the purpose of using the late Miocene to inform potential future climate changes, the locations that should be targeted for palaeodata acquisition are those which are most sensitive to CO_2 forcing (because a large signal-to-noise ratio is required to overcome the uncertainties in palaeodata reconstructions), but where the difference between the simulated modern climate and the late Miocene climates is smallest because these are the regions which are most insensitive to the geographic configuration. By using the difference between the late Miocene $C400_{TRIF}$ and $C280_{TRIF}$ simulations and overlaying as a mask the 'no difference' between the late Miocene and the potential modern simulations (effectively exposing only Figure 2A through the white areas from Figure 2E, but for the annual mean and the cold month and warm month means), these model results suggest that some of the currently available southern European and central Asian late Miocene data are suitable for this purpose (see Supplementary Figure S18). Other regions, where data are currently lacking, include North America, northern Africa, Australia, Paraguay and southern Brazil, and northeastern Asia. Note however, that for some localities tectonic movement has been significant between the late Miocene and today, e.g. in Australia, but that this movement has not been incorporated into the results presented here.

4 Conclusions

A series of CO_2 and vegetation perturbation experiments have been conducted under late Miocene and modern boundary conditions. At the lowest CO_2 (180ppm), the late Miocene palaeogeography and vegetation distributions produce a simulated global mean annual temperature and precipitation which is very similar to the climate simulated with the modern geography and vegetation distribution. The model simulations presented here agree with previous assessments that the late Miocene was globally warmer and wetter for CO_2

concentrations greater than 180ppm (Bradshaw et al., 2012; Knorr et al., 2011; Micheels et al., 2009; Micheels et al., 2011; Micheels et al., 2007). The magnitude of the difference remains difficult to ascertain due to uncertainty in late Miocene soil parameters, which we suggest might increase the late Miocene global mean annual temperature by up to 0.5°C. Future work should include reconstructing late Miocene soil parameters to enable better model representation of late Miocene conditions, as has recently been done for the Pliocene (Pound et al., 2013) and the middle Miocene (Metzger, 2013).

As CO_2 is increased from 180 to 280ppm and 280 to 400ppm, both sets of boundary conditions lead to a poleward shift in shrub and tree cover in the Northern Hemisphere and a reduction in the size of the Amazon Rainforest and southern African forests. Separation of the direct CO_2 forcing and the vegetation changes for the late Miocene reveals that increasing CO_2 alone results in the greatest warming being expressed at high latitudes during the respective winter months but CO_2 forcing cannot alone account for all of the warming seen in the control simulations; the contribution of the vegetation change is significant and can be up to 7°C across the mid-high northern latitudes (for the 180 to 280ppm CO_2 change; not shown). Our results suggest that vegetation feedbacks are important; climate model simulations that do not include vegetation feedbacks will significantly underestimate warming due to increasing CO_2. Therefore our model results can be considered to lie between the traditional definition of Climate Sensitivity which considers only fast feedbacks, and Earth System Sensitivity which considers fast and slow feedbacks such as vegetation changes (e.g. Lunt et al., 2010), but not a full representation of Earth System Sensitivity because our continental ice sheet configuration is fixed across the CO_2 concentrations simulated. However, since our vegetation model is biophysical only it does not incorporate vegetation

CO_2 feedbacks to the atmosphere which are also very important. For example, it is estimated that the European terrestrial biosphere absorbed 7-12% of the 1995 anthropogenic carbon emissions (Janssens et al., 2003) whereas in our study the CO_2 concentration is unaltered by the vegetation distribution changes made; there is no biochemical feedback. Vegetation modelling studies carried out by Francois et al. (2006) find that the total global terrestrial carbon stock of the late Miocene would be 159Gt greater than the present day under preindustrial levels of CO_2 and that the late Miocene would experience an increase of 1727Gt for a CO_2 doubling.

The model-derived contribution to the warming from CO_2 forcing alone and the contribution to the warming from vegetation changes do not add linearly. Considering a change from low to high CO_2, in some regions the synergy is positive and the temperature response to CO_2 forcing is amplified, but mostly the temperature synergy is negative and acts to dampen the temperature response to CO_2 forcing. This occurs most strongly in regions where sea ice concentrations reduce and is therefore related to changes in the sea ice-albedo feedback mechanism. Differences in the sign and magnitude of synergy in the Southern Hemisphere between simulations with the late Miocene and the modern boundary conditions are suggested to result from the different ocean circulation that occurs with the late Miocene boundary conditions and the fact that Northern Hemisphere-derived vegetation changes are not translated to the Southern Hemisphere. Precipitation synergy is both negative and positive with complex spatial patterns, but global annual synergy is also negative. Regions that are most different in their sensitivity to increasing CO_2 between the late Miocene boundary conditions and the modern boundary conditions are those which undergo the most significant palaeogeographical alteration, e.g. the Bering Strait, the Barents/Kara Sea and the Hudson

Bay region. However, the uncertainties in the palaeogeography itself must also be considered and so future work should investigate the sensitivity of the results presented here to different tectonic configurations for the late Miocene. Additionally, it is stressed that presented here are the results from a single model, and the climate sensitivities derived are towards the upper end of the range of climate sensitivities determined from the CMIP5 models (Stocker et al., 2013), implying that other models may suggested reduced climate changes for the same CO_2 changes made in this study.

Comparisons of the model results to the quantitative terrestrial palaeorecord show that for the majority of the data (located in Europe and central Asia), the mean annual temperatures, the cold month mean temperatures and the warm month mean temperatures best fit with the 400ppm CO_2 concentration simulation with the 400ppm vegetation distribution. However, the mean annual precipitations best fit with the 180ppm CO_2 concentration simulation with the 180ppm vegetation distribution. The reasons for this discrepancy remain open. In order to test the regions of poor model-data comparison, Late Miocene sensitivity studies of the configuration of the North American Cordillera, the Panama Gateway, the Bering Strait, the Barents/Kara Sea, the Himalayas and the Indonesian Seaway are recommended because these are the regions of most palaeogeographic change, as well as fixed late Miocene vegetation simulations using PFT representations of the biome reconstructions of Pound et al. (2011, 2012).

This work shows that palaeogeography is important for determining the vegetation distribution at high latitudes and this has a significant effect on the climate sensitivity of the late Miocene. The model results suggest that climate sensitivity to CO_2 forcing is directly affected by the palaeogeographic configuration and that globally the late Miocene was 0.5-

0.8°C more sensitive to CO_2 forcing than we might expect future climate to be because of the greater land mass at high northern latitudes during the late Miocene and the different vegetation distribution predictions that result. At high northern latitudes, the late Miocene palaeogeography consists of a near ice-free Greenland, a closed Bering Strait and a landmass where the Barents and Kara Seas reside today. Whilst future climate may include further reductions in the size of the Greenland Ice Sheet, which could make available additional vegetated land, the Barents/Kara Sea landmass will not be available again and the Bering Strait may only close on orbital timescales.

Our modelling suggests that the optimal regions to target late Miocene palaeodata acquisition for the purposes of informing future climate are North America, northern Africa, Australia, Paraguay and southern Brazil, and northeastern Asia. These are the regions that the model results predict to be most sensitive to CO_2 forcing, but where the palaeogeographic differences do not significantly influence the local temperature response.

In conclusion, if modern climate were to reach equilibrium with present day CO_2 concentrations (400ppm) we might expect the climate to become globally warmer and wetter, however, model results suggest that it is unlikely to be as warm or wet as the late Miocene for that same CO_2 concentration. This is because the paleogeography of the late Miocene and the resultant vegetation differences make the climate more sensitive to CO_2 forcing due to differences in the combination of sea ice, cloud, and ocean circulation feedbacks.

5 Acknowledgements

This work was carried out using the computing facilities of the Advanced Computing Research Centre at the University of Bristol, http://www.bris.ac.uk/acrc. Catherine Bradshaw and Taraka Davies-Barnard are funded by NERC PhD studentships.

6 References

Ainsworth, E.A., Rogers, A., 2007. The response of photosynthesis and stomatal conductance to rising CO2: mechanisms and environmental interactions. Plant, Cell & Environment 30, 258-270.

Alo, C.A., Wang, G., 2008. Potential future changes of the terrestrial ecosystem based on climate projections by eight general circulation models. Journal of Geophysical Research: Biogeosciences 113, G01004.

Álvarez-Solas, J., Montoya, M., Ritz, C., Ramstein, G., Charbit, S., Dumas, C., Nisancioglu, K., Dokken, T., Ganopolski, A., 2011. Heinrich event 1: an example of dynamical ice-sheet reaction to oceanic changes. Clim. Past 7, 1297-1306.

Berry, J.A., Downton, W.J.S., 1982. Environmental regulation of photosynthesis. Photosynthesis 2, 263-343.

Billups, K., Ravelo, A.C., Zachos, J.C., Norris, R.D., 1999. Link between oceanic heat transport, thermohaline circulation, and the Intertropical Convergence Zone in the early Pliocene Atlantic. Geology 27, 319-322.

Blanc, P.L., Rabussier, D., Vergnaudgrazzini, C., Duplessy, J.C., 1980. North-Atlantic Deep-Water Formed by the Later Middle Miocene. Nature 283, 553-555.

Bogaert, J., Zhou, L., Tucker, C.J., Myneni, R.B., Ceulemans, R., 2002. Evidence for a persistent and extensive greening trend in Eurasia inferred from satellite vegetation index data. Journal of Geophysical Research: Atmospheres 107, ACL 4-1-ACL 4-14.

Bonan, G.B., 2008. Forests and climate change: Forcings, feedbacks, and the climate benefits of forests. Science 320, 1444-1449.

Bradshaw, C.D., Lunt, D.J., Flecker, R., Salzmann, U., Pound, M.J., Haywood, A.M., Eronen, J.T., 2012. The relative roles of CO2 and palaeogeography in determining Late Miocene climate: results from a terrestrial model-data comparison. Climates of the Past Discussions 8, 715-786.

Bruch, A.A., Uhl, D., Mosbrugger, V., 2007. Miocene climate in Europe - Patterns and evolution - A first synthesis of NECLIME. Palaeogeography Palaeoclimatology Palaeoecology 253, 1-7.

Carson, D.J., Sangster, A.B., 1981. The influence of landsurface albedo and soil moisture on general circulation model simulations. , in: Rutherford, I.D. (Ed.), GARP/WCRP: Research Activities in Atmospheric and Oceanic Modeling., pp. 5.14–15.21.

Cox, P.M., Betts, R.A., Jones, C.D., Spall, S.A., Totterdell, I.J., 2000. Acceleration of global warming due to carbon-cycle feedbacks in a coupled climate model. Nature 408, 184-187.

Cramer, W., Bondeau, A., Woodward, F.I., Prentice, I.C., Betts, R.A., Brovkin, V., Cox, P.M., Fisher, V., Foley, J.A., Friend, A.D., Kucharik, C., Lomas, M.R., Ramankutty, N., Sitch, S., Smith, B., White, A., Young-Molling, C., 2001. Global response of terrestrial ecosystem structure and function to CO2 and climate change: results from six dynamic global vegetation models. Global Change Biology 7, 357-373.

D'Arrigo, R., Jacoby, G.C., Fung, I.Y., 1987. Boreal forests and atmosphere-biosphere exchange of carbon dioxide. Nature 329, 321-323.

Delaney, M.L., 1990. Miocene benthic foraminiferal Cd/Ca records: South Atlantic and western equatorial Pacific. Paleoceanography 5, 743-760.

Demicco, R.V., Lowenstein, T.K., Hardie, L.A., 2003. Atmospheric *p*CO2 since 60 Ma from records of seawater pH, calcium, and primary carbonate mineralogy. Geology 31, 793-796.

Dirmeyer, P.A., Shukla, J., 1994. Albedo as a modulator of climate response to tropical deforestation. J Geophys Res 99, 20863-20820,20877.

Eltahir, E.A., 1998. A soil moisture–rainfall feedback mechanism: 1. Theory and observations. Water Resour Res 34, 765-776.

Emanuel, W., Shugart, H., Stevenson, M., 1985. Climatic change and the broad-scale distribution of terrestrial ecosystem complexes. Climatic Change 7, 29-43.

Eronen, J.T., Puolamäki, K., Liu, L., Lintulaakso, K., Damuth, J., Janis, C., Fortelius, M., 2010. Precipitation and large herbivorous mammals , part II: Application to fossil data. Evol Ecol Res 12, 235-248.

Farquhar, G.D., Sharkey, T.D., 1982. Stomatal conductance and photosynthesis. Annual review of plant physiology 33, 317-345.

Findell, K.L., Eltahir, E.A., 1997. An analysis of the soil moisture-rainfall feedback, based on direct observations from Illinois. Water Resour Res 33, 725-735.

Foster, G.L., Lunt, D.J., Parrish, R.R., 2010. Mountain uplift and the glaciation of North America - a sensitivity study. Climate of the Past 6, 707-717.

Francois, L., Ghislain, M., Otto, D., Micheels, A., 2006. Late Miocene vegetation reconstruction with the CARAIB model. Palaeogeography Palaeoclimatology Palaeoecology 238, 302-320.

Freeman, K.H., Hayes, J.M., 1992. Fractionation of carbon isotopes by phytoplankton and estimates of ancient CO2 levels. Global Biogeochemical Cycles 6, 185-198.

Ganopolski, A., Kubatzki, C., Claussen, M., Brovkin, V., Petoukhov, V., 1998. The influence of vegetation-atmosphere-ocean interaction on climate during the mid-Holocene. Science 280, 1916-1919.

Gerber, S., Joos, F., Prentice, I.C., 2004. Sensitivity of a dynamic global vegetation model to climate and atmospheric CO2. Global Change Biology 10, 1223-1239.

Gordon, C., Cooper, C., Senior, C.A., Banks, H., Gregory, J.M., Johns, T.C., Mitchell, J.F.B., Wood, R.A., 2000. The simulation of SST, sea ice extents and ocean heat transports in a version of the Hadley Centre coupled model without flux adjustments. Climate Dynamics 16, 147-168.

Haug, G.H., Tiedemann, R., 1998. Effect of the formation of the Isthmus of Panama on Atlantic Ocean thermohaline circulation. Nature 393, 673-676.

Janssens, I.A., Freibauer, A., Ciais, P., Smith, P., Nabuurs, G.-J., Folberth, G., Schlamadinger, B., Hutjes, R.W., Ceulemans, R., Schulze, E.-D., 2003. Europe's terrestrial biosphere absorbs 7 to 12% of European anthropogenic CO2 emissions. Science 300, 1538-1542.

Joos, F., Prentice, I.C., Sitch, S., Meyer, R., Hooss, G., Plattner, G.-K., Gerber, S., Hasselmann, K., 2001. Global warming feedbacks on terrestrial carbon uptake under the Intergovernmental Panel on Climate Change (IPCC) Emission Scenarios. Global Biogeochemical Cycles 15, 891-907.

Keller, G., Barron, J.A., 1983. Paleoceanographic Implications of Miocene Deep-Sea Hiatuses. Geological Society of America Bulletin 94, 590-613.

Knorr, G., Butzin, M., Micheels, A., Lohmann, G., 2011. A warm Miocene climate at low atmospheric CO2 levels. Geophys Res Lett 38, L20701.

Kurschner, W.M., Kvacek, Z., Dilcher, D.L., 2008. The impact of Miocene atmospheric carbon dioxide fluctuations on climate and the evolution of terrestrial ecosystems. Proceedings of the National Academy of Sciences of the United States of America 105, 449-453.

Kurschner, W.M., vanderBurgh, J., Visscher, H., Dilcher, D.L., 1996. Oak leaves as biosensors of late Neogene and early Pleistocene paleoatmospheric CO2 concentrations. Marine Micropaleontology 27, 299-312.

Levis, S., Bonan, G.B., Bonfils, C., 2004. Soil feedback drives the mid-Holocene North African monsoon northward in fully coupled CCSM2 simulations with a dynamic vegetation model. Climate Dynamics 23, 791-802.

Loptson, C.A., Lunt, D.J., and Francis, J.E. 2014. Investigating vegetation-climate feedbacks during the early Eocene. Climates of the Past 10, 419-436

Lucht, W., Prentice, I.C., Myneni, R.B., Sitch, S., Friedlingstein, P., Cramer, W., Bousquet, P., Buermann, W., Smith, B., 2002. Climatic Control of the High-Latitude Vegetation Greening Trend and Pinatubo Effect. Science 296, 1687-1689.

Lunt, D.J., Flecker, R., Clift, P.D., 2010. The impacts of Tibetan uplift on palaeoclimate proxies. Geological Society of London, Special Publications 342, 279-291.

Lunt, D.J., Haywood, A.M., Schmidt, G.A., Salzmann, U., Valdes, P.J., Dowsett, H.J., 2010. Earth system sensitivity inferred from Pliocene modelling and data. Nature Geoscience 3, 60-64.

Lunt, D.J., Haywood, A.M., Schmidt, G.A., Salzmann, U., Valdes, P.J., Dowsett, H.J., Loptson, C.A., 2012. On the causes of mid-Pliocene warmth and polar amplification. Earth and Planetary Science Letters 321, 128-138.

Markwick, P.J., 2007. The palaeogeographic and palaeoclimatic significance of climate proxies for data-model comparisons. Deep-Time Perspectives on Climate Change: Marrying the Signal from Computer Models and Biological Proxies, 251-312.

Metzger, C., 2013. Miocene Soil Database: Global paleosol and climate maps of the Middle Miocene Thermal Maximum, American Geopysical Union Fall Meeting, San Francisco.

Micheels, A., Bruch, A., Mosbrugger, V., 2009. Miocene Climate Modelling Sensitivity Experiments for Different CO2 Concentrations. Palaeontol Electron 12, -.

Micheels, A., Bruch, A.A., Eronen, J., Fortelius, M., Harzhauser, M., Utescher, T., Mosbrugger, V., 2011. Analysis of heat transport mechanisms from a Late Miocene model experiment with a fully-coupled atmosphere-ocean general circulation model. Palaeogeography, Palaeoclimatology, Palaeoecology In Press, Corrected Proof.

Micheels, A., Bruch, A.A., Uhl, D., Utescher, T., Mosbrugger, V., 2007. A Late Miocene climate model simulation with ECHAM4/ML and its quantitative validation with terrestrial proxy data. Palaeogeography Palaeoclimatology Palaeoecology 253, 251-270.

Miller, K.G., Fairbanks, R.G., 1985. Oligocene to Miocene carbon isotope cycles and abyssal circulation changes. The Carbon Cycle and Atmospheric CO: Natural Variations Archean to Present, 469-486.

Mintz, Y., 1984. The sensitivity of numerically simulated climates to land surface conditions. The global climate.

Myneni, R.B., Keeling, C., Tucker, C., Asrar, G., Nemani, R., 1997. Increased plant growth in the northern high latitudes from 1981 to 1991. Nature 386, 698-702.

Oglesby, R.J., Erickson III, D.J., 1989. Soil moisture and the persistence of North American drought. Journal of Climate 2, 1362-1380.

Pagani, M., Arthur, M.A., Freeman, K.H., 1999a. Miocene evolution of atmospheric carbon dioxide. Paleoceanography 14, 273-292.

Pagani, M., Freeman, K.H., Arthur, M.A., 1999b. Late Miocene atmospheric CO2 concentrations and the expansion of C-4 grasses. Science 285, 876-879.

Pagani, M., Liu, Z., LaRiviere, J., Ravelo, A.C., 2010. High Earth-system climate sensitivity determined from Pliocene carbon dioxide concentrations. Nature Geoscience 3, 27-30.

Pearson, P.N., Palmer, M.R., 2000. Atmospheric carbon dioxide concentrations over the past 60 million years. Nature 406, 695-699.

Pope, V.D., Gallani, M.L., Rowntree, P.R., Stratton, R.A., 2000. The impact of new physical parametrizations in the Hadley Centre climate model: HadAM3. Climate Dynamics 16, 123-146.

Pound, M.J., Haywood, A.M., Salzmann, U., Riding, J.B., 2012. Global vegetation dynamics and latitudinal temperature gradients during the Mid to Late Miocene (15.97–5.33Ma). Earth-Sci Rev 112, 1-22.

Pound, M.J., Haywood, A.M., Salzmann, U., Riding, J.B., Lunt, D.J., Hunter, S.J., 2011. A Tortonian (Late Miocene, 11.61-7.25 Ma) global vegetation reconstruction. Palaeogeography Palaeoclimatology Palaeoecology 300, 29-45.

Pound, M.J., Tindall, J., Pickering, S.J., Haywood, A.M., Dowsett, H.J., Salzmann, U., 2013. Late Pliocene lakes and soils: a data-model comparison for the analysis of climate feedbacks in a warmer world. Clim. Past Discuss. 9, 3175-3207.

Rohling, E., Sluijs, A., Dijkstra, H., Köhler, P., van de Wal, R., von der Heydt, A., Beerling, D., Berger, A., Bijl, P., Crucifix, M., 2012. Making sense of palaeoclimate sensitivity. Nature 491, 683-691.

Salazar, L.F., Nobre, C.A., Oyama, M.D., 2007. Climate change consequences on the biome distribution in tropical South America. Geophys Res Lett 34, L09708.

Scholze, M., Knorr, W., Arnell, N.W., Prentice, I.C., 2006. A climate-change risk analysis for world ecosystems. Proceedings of the National Academy of Sciences 103, 13116-13120.

Seneviratne, S.I., Corti, T., Davin, E.L., Hirschi, M., Jaeger, E.B., Lehner, I., Orlowsky, B., Teuling, A.J., 2010. Investigating soil moisture–climate interactions in a changing climate: a review. Earth-Sci Rev 99, 125-161.

Solomon, A., 1986. Transient response of forests to CO2-induced climate change: simulation modeling experiments in eastern North America. Oecologia 68, 567-579.

Stärz, M., Lohmann, G., Knorr, G., 2013. Dynamic soil feedbacks on the climate of the mid-Holocene and the Last Glacial Maximum. Clim. Past Discuss. 9, 2717-2770.

Stocker, T.F., Qin, D., Plattner, G.-K., Tignor, M., Allen, S.K., Boschung, J., Nauels, A., Xia, Y., Bex, V., Midgley, P.M., 2013. Climate Change 2013. The Physical Science Basis. Working Group I Contribution to the Fifth Assessment Report of the Intergovernmental Panel on Climate Change-Abstract for decision-makers. Groupe d'experts intergouvernemental sur l'evolution du climat/Intergovernmental Panel on Climate Change-IPCC, C/O World Meteorological Organization, 7bis Avenue de la Paix, CP 2300 CH-1211 Geneva 2 (Switzerland).

Swann, A.L., Fung, I.Y., Chiang, J.C., 2012. Mid-latitude afforestation shifts general circulation and tropical precipitation. Proceedings of the National Academy of Sciences 109, 712-716.

Tiedemann, R., Franz, S.O., 1997. Deep-water circulation, chemistry, and terrigenous sediment supply in the Equatorial Atlantic during the Pliocene, 3.3-2.6 Ma and 5-4.5 Ma, in: Shackleton, N.J., Curry, W.B., Richter, C., Bralower, T.J. (Eds.), Proceedings of the Ocean Drilling Program, Scientific Results. Texas A & M University, Ocean Drilling Program, College Station, TX, pp. 299-318.

Tripati, A.K., Roberts, C.D., Eagle, R.A., Li, G., 2011. A 20 million year record of planktic foraminiferal B/Ca ratios: Systematics and uncertainties in pCO2 reconstructions. Geochim Cosmochim Ac 75, 2582-2610.

Utescher, T., Böhme, M., Mosbrugger, V., 2011. The Neogene of Eurasia: Spatial gradients and temporal trends — The second synthesis of NECLIME. Palaeogeography, Palaeoclimatology, Palaeoecology 304, 196-201.

Woodruff, F., Savin, S.M., 1989. Miocene deepwater oceanography. Paleoceanography 4, 87-140.

Wright, J.D., Miller, K.G., Fairbanks, R.G., 1992. Early and middle Miocene stable isotopes: Implications for deepwater circulation and climate. Paleoceanography 7, 357-389.

Zhang, Y.G., Pagani, M., Liu, Z., Bohaty, S.M., DeConto, R., 2013. A 40-million-year history of atmospheric CO2. Philosophical Transaction of the Royal Society A in press.

Zhou, J., Poulsen, C., Rosenbloom, N., Shields, C., Briegleb, B., 2012. Vegetation-climate interactions in the warm mid-Cretaceous. Climate of the Past 8, 565-576.

Figure 1. Schematic showing the evolution of the late Miocene and potential modern GCM runs used in this study. All of the runs have been conducted with late Miocene boundary conditions; the asterisks indicate which of the run combinations have also been conducted with modern boundary conditions. For clarity the reader is referred to the online version of this paper where a colour version of this figure is provided.

Figure 2. Temperature and precipitation changes due to CO_2 forcing including vegetation changes. Shown are the results for changing CO_2 from 280ppm to 400ppm. Only significant differences are shown using a 95% confidence interval Student's T-Test; white areas are not significant. For the righthand panels, both land-sea masks are shown; the modern land-sea mask is dotted. For clarity the reader is referred to the online version of this paper where a colour version of this figure is provided.

Figure 3. Fractional changes in vegetation distribution due to CO_2 forcing under late Miocene boundary conditions as predicted by the TRIFFID model. Left hand panels are anomalies of the 280ppm simulations with the 180ppm simulations. Middle panels are anomalies of the 400ppm simulations with the 280ppm simulations. Right hand panels show the latitudinal

distribution in vegetation for each of the three CO_2 concentrations. For clarity the reader is referred to the online version of this paper where a colour version of this figure is provided.

Figure 4. Fractional changes in vegetation distribution due to CO_2 forcing under modern boundary conditions as predicted by the TRIFFID model. Left hand panels are anomalies of the 280ppm simulations with the 180ppm simulations. Middle panels are anomalies of the 400ppm simulations with the 280ppm simulations. Right hand panels show the latitudinal distribution in vegetation for each of the three CO_2 concentrations. For clarity the reader is referred to the online version of this paper where a colour version of this figure is provided.

Figure 5. Global changes in the dominant vegetation distributions as simulated by the TRIFFID vegetation model under the three CO_2 scenarios: 180ppm, 280ppm and 400ppm for the late Miocene (LM) and the modern (PM) boundary conditions. For clarity the reader is referred to the online version of this paper where a colour version of this figure is provided.

Figure 6. Dominant vegetation distributions as simulated by the TRIFFID vegetation model under the three CO_2 scenarios: 180ppm, 280ppm and 400ppm for the late Miocene and the Modern boundary conditions. For clarity the reader is referred to the online version of this paper where a colour version of this figure is provided.

Figure 7. Lefthand column: Near-surface air temperature and precipitation changes due to CO_2 forcing alone (excluding vegetation changes; Equation 1). Righthand side: Near-surface air temperature and precipitation changes due to vegetation changes alone (excluding direct

CO_2 forcing; Equation 2). Panels A-D and I-L show the late Miocene boundary condition results, panels E-H and M-P show the modern boundary condition results. Shown are the contributions as a result of increasing from 280 to 400ppm, but the results for increasing from 180 to 280ppm are very similar. Only significant differences are shown using a 95% confidence interval Student's T-Test; white areas are not significant. For clarity the reader is referred to the online version of this paper where a colour version of this figure is provided.

Figure 8. Synergy between the direct CO_2 forcing and the vegetation feedbacks (Equation 3). The top four panels show the synergy for the mean annual temperature and the bottom four panels show the synergy for the mean annual precipitation. Displayed are the results for changing CO_2 from 280ppm to 400ppm whilst the vegetation is fixed at the distribution in equilibrium with the ambient CO_2. If the contributions from direct CO_2 forcing and from vegetation changes add linearly, the anomalies will be zero. For clarity the reader is referred to the online version of this paper where a colour version of this figure is provided.

Figure 9. Global mean annual near-surface air temperature (A) and precipitation (B) sensitivity to CO_2 concentration (including vegetation feedbacks).

Figure 10. Change in sea ice concentration for a CO_2 change from 280ppm to 400ppm with vegetation feedbacks included ($C400_{TRIF} – C280_{TRIF}$). For clarity the reader is referred to the online version of this paper where a colour version of this figure is provided.

Figure 11. Improvements in the model-data comparison due to vegetation changes and due to the CO_2 changes. Green circles indicate an improvement, red circles indicate deterioration. The datapoints showing 'no difference' are plotted underneath the other datapoints in order to highlight the differences. For clarity the reader is referred to the online version of this paper where a colour version of this figure is provided.

Figure 12. The best-fit scenarios to the data. For the top row, A and D (G and J) show which CO_2 (vegetation) scenario is closest to the data reconstructions when the vegetation distribution (CO_2) imposed is 180ppm. The middle row, B and E (H and K) show which CO_2 (vegetation) scenario is closest to the data reconstructions when the vegetation (CO_2) imposed is 280ppm. The bottom row C and F (I and L) show which CO_2 (vegetation) scenario is closest to the data reconstructions when the vegetation (CO_2) imposed is 400ppm. The datapoints for which there is no discernible difference in the model-data comparison between all of the CO_2 scenarios (i.e. they all overlap with the data) are shown in white and are plotted underneath the other datapoints in order to highlight the differences. For clarity the reader is referred to the online version of this paper where a colour version of this figure is provided.

Table 1. Factor separation of CO_2 forcing and vegetation changes and the synergy calculated from non-linearity between the two. f_{CO2} is the contribution from CO_2 forcing, f_{VEG} is the contribution from the vegetation changes and f_{SYN} is the synergy term defined as going from the lower CO_2 to the higher CO_2.

Table 2. Inferred equilibrium climate sensitivity for the late Miocene and modern boundary conditions. Numbers are obtained by scaling the output from the simulations presented in this work to that for a standard climate sensitivity definition of the global mean near-surface air temperature change for a doubling of CO_2 (using scaling factors of 1.57 for the 180 to 280ppm CO_2 change and 1.94 for the 280ppm to 400ppm CO_2 change (Lunt et al., 2010)). For the modern simulations, results from the homogenous soils experiments are shown in parentheses.

Table 3. Inferred equilibrium climate sensitivity and the contribution from vegetation changes. Numbers are obtained by scaling the output from the simulations presented in this work to that for a standard climate sensitivity definition of the global mean temperature change for a doubling of CO_2 (using scaling factors of 1.57 for the 180 to 280ppm CO_2 change and 1.94 for the 280ppm to 400ppm CO_2 change (Lunt et al., 2010)).

Supplementary Information

S1. Dynamic vegetation model TRIFFID

The interactive global vegetation model coupled to HadCM3L is the Top-down Representation of Interactive Foliage and Flora Including Dynamics (TRIFFID) model, a full description of which is given in Cox, (2001) and Hughes et al. (2004). TRIFFID has been found to be dynamically stable and that the variations in the modelled vegetation distributions are driven by perturbations in the atmosphere (Hughes et al., 2006).

TRIFFID calculates areal coverage, leaf area index and canopy height for five defined plant functional types (PFTs): broadleaf tree, needleleaf tree, C_3 grass, C_4 grass and shrub. These PFTs respond differently to climate and CO_2 forcing (e.g. C_3 and C_4 grasses use different photosynthetic pathways), and also impact differently on the physical properties of the land surface (i.e. possessing different aerodynamic roughness lengths and albedo properties). All PFTs can co-exist within the same gridbox, each possessing a fractional coverage that is equivalent to the population size. The fractional coverage co-existence approach allows smooth transitions to occur when the vegetation distribution changes rather than the sudden discontinuities that would occur in a 'dominant' PFT only approach (Svirezhev, 2000).

The MOSES2 scheme calculates the net primary productivity (NPP) as the difference between photosynthesis and respiration for each PFT, and this quantity is then converted into the biomass for each PFT per unit area together with a component of spreading, which results in changes in the fractional distribution for that PFT. Light competition from other PFTs interferes with the spreading. Tree PFTs compete in relation to their canopy heights, as do grass PFTs and a simple dominance hierarchy between tree-shrub-grass determines the competition between trees, grasses and shrubs (Betts et al., 2004). Disturbance such as that due to disease and fire, can be represented by a single disturbance rate for a given PFT but the effect of these impacts is beyond the scope of this study and so no disturbance to PFTs is assumed here.

The NPP is calculated by a coupled photosynthesis-stomatal conductance model (Cox et al., 1998). Factors affecting the rate of photosynthesis are the humidity deficit, the photochemically active radiation, soil moisture and leaf area index. The maximum rate of photosynthesis is directly related to the leaf temperature and the upper and lower temperatures for photosynthesis (defined individually for each PFT). The PFTs compete horizontally in that grasses replace bare soil, shrubs replace grasses and trees replace shrubs.

The predicted vegetation in each grid box feeds back into the climate system in a number of ways, principally through evapotranspiration from the canopy, alteration of surface albedo, and through alteration of mixing at the boundary layer between the surface and the atmosphere (roughness length), selected parameters used in the model for each PFT are given in Table S1. Evaporation from transpiring vegetation is calculated using a photosynthesis model with climatic variables, soil moisture and the vegetation type (Cox et al. 1998; Cox 2001). The surface albedo is based on the fractions of each PFT, the fraction of snow-cover and a prescribed albedo for that PFT, both snow-free and snow-covered. The prescribed albedos are based on the canopy radiative transfer model of Sellers (1985). The roughness length is calculated according to the modelled height of the vegetation and a parameter corresponding to the rate of change of vegetation roughness length with height, separately defined for each PFT. The roughness length of vegetation is incorporated into the albedo calculations when snow covered, e.g. a forested grid box is given a lower albedo than a shrub or grass filled grid box with the same depth of snow cover. The roughness length of a grid box will contribute to the determination of the sensible heat and moisture fluxes, and also the near surface wind speed.

Parameter	Broadleaf Tree	Needleleaf Tree	C3 Grass	C4 Grass	Shrub
Initial canopy height	19.0	16.38	0.8	1.26	2.0
Initial leaf area index	5.0	4.0	2.0	4.0	2.5
Initial canopy conductance	0.014	0.014	0.014	0.014	0.014
Temperature below which leaves are dropped	0	-30	-15	-15	-30
Lower temperature for photosynthesis	0.0	-5.0	0.0	13.0	0.0
Upper temperature for photosynthesis	36.0	31.0	36.0	45.0	36.0
Critical humidity deficit	0.09	0.06	0.10	0.075	0.10
Snow-covered albedo for large LAI	0.15	0.15	0.60	0.60	0.40
Snow-covered albedo for zero LAI	0.30	0.30	0.80	0.80	0.80
Snow-free albedo for large LAI	0.10	0.10	0.20	0.20	0.20
Rate of change of roughness length with height	0.05	0.05	0.10	0.10	0.10
Rootdepth (m)	3.00	1.00	0.50	0.50	0.50

Table S1. Selected TRIFFID PFT parameters

Two modes of coupling between the TRIFFID and the GCM are possible: a spinup equilibrium mode in which the fluxes between the land and the atmosphere are calculated by the GCM and averaged over ~5 years, and a more computationally demanding dynamic mode, which is used to incorporate the seasonal cycle with the fluxes calculated on every 30 minute timestep and averaged over 10 days. The averaged fluxes are then passed to TRIFFID which calculates the growth and expansion of the existing vegetation, and updates the land surface parameters based on the new vegetation distribution and structure.

It is important to note that it is not a necessity for the vegetation structure to be in equilibrium with the climate: modelled vegetation may lag the status of the climate and in many cases it has been well documented that vegetation is not sensitive to short timescale variability (Henderson-Sellers, 1993; Woodward et al., 1998), and significant disequilibrium has been observed, e.g. for European tree distributions (Svenning and Skov, 2004). The work of Hughes et al. (2006) suggests that there are substantial lags associated with TRIFFID components, and that simulations should be run for more than 300 years in order to reach vegetative equilibrium.

The TRIFFID model has been compared to IGBP-DIS land cover dataset (Loveland and Belward, 1997), which represents the modern distribution of vegetation as derived from satellite image interpretation (Betts et al., 2004). This suggests that the shrub PFT is overestimated at high latitudes at the expense of forests, perhaps as a result of the high latitude cold bias in the GCM. The broadleaf tree PFT is also overestimated in equatorial regions, with the exception of at the mouth of the River Amazon where model underestimated precipitation leads to TRIFFID modelling the presence of C4 grasses instead of broadleaf trees. Grasses tend to be globally slightly underestimated with the position of vegetation in the Sahara desert and other arid regions well reproduced, but the density is modelled to be too sparse, particularly in south-west Africa, central and south-west Asia, south-west North America and Australia. The discrepancies between the satellite imagery and the TRIFFID model are suggested to be a combination of orographic representation leading to underestimation of precipitation, differences between the anthropogenic masks used in the model and that found on the satellite imagery, and the inadequate treatment of natural disturbance mechanisms such as fire (Betts et al., 2004).

Although there are six vegetation definitions output from TRIFFID (broadleaf trees, needleleaf trees, C_3 grass, C_4 grass, shrubs and bare soil), the PFT albedos used in the model are identical between broadleaf and needleleaf trees and between C_3 and C_4 grasses, and there are no differences in the parameters that determine the roughness length between broadleaf and needleleaf trees, and between C_3 and C_4 grasses. Therefore, although not completely identical, to ease the analysis we consider the results in terms of only four landcover types: trees, grasses, shrubs and bare soil under the general assumption that the potential contribution to the climate from the two tree types are extremely similar and also between the two grass types, but that their actual contribution (the fraction and distribution of each PFT in each gridbox as determined by firstly by climatic thresholds and subsequently by the competition hierarchy between the trees, grasses and shrubs) will be accounted for by their location, i.e. needleleaf trees and C_3 grasses at higher latitudes, broadleaf and C_4 grasses at lower latitudes, and a mix in mid latitudes.

S2. Experimental Design

S2.1 Late Miocene Boundary Conditions

The geological record provides evidence for an palaeogeographic configuration during the late Miocene that was distinctly different to today including an open Panama Gateway (Duque-Caro, 1990; Keigwin, 1982), an unrestricted Indonesian Seaway (Cane and Molnar, 2001; Edwards, 1975; Kennett et al., 1985; van Andel et al., 1975), a closed Bering Strait (Gladenkov et al., 2002; Marincovich Jr and Gladenkov, 2001; Marincovich and Gladenkov, 1999). On land the palaeorecord suggests major uplift of the Himalayas (Fang et al., 2005; Harrison et al., 1992; Molnar et al., 1993; Rowley and Currie, 2006), the Andes (Garzione et al., 2008; Gregory-Wodzicki, 2002), the North American Rockies (Morgan and Swanberg, 1985), the East African Plateaus (Saggerson and Baker, 1965; Yemane et al., 1985), and the Alps (Kuhlemann, 2007; Spiegel et al., 2001) during the late Miocene. Figure S1 details the boundary condition used in our late Miocene simulations and highlights the major differences to the modern geography.

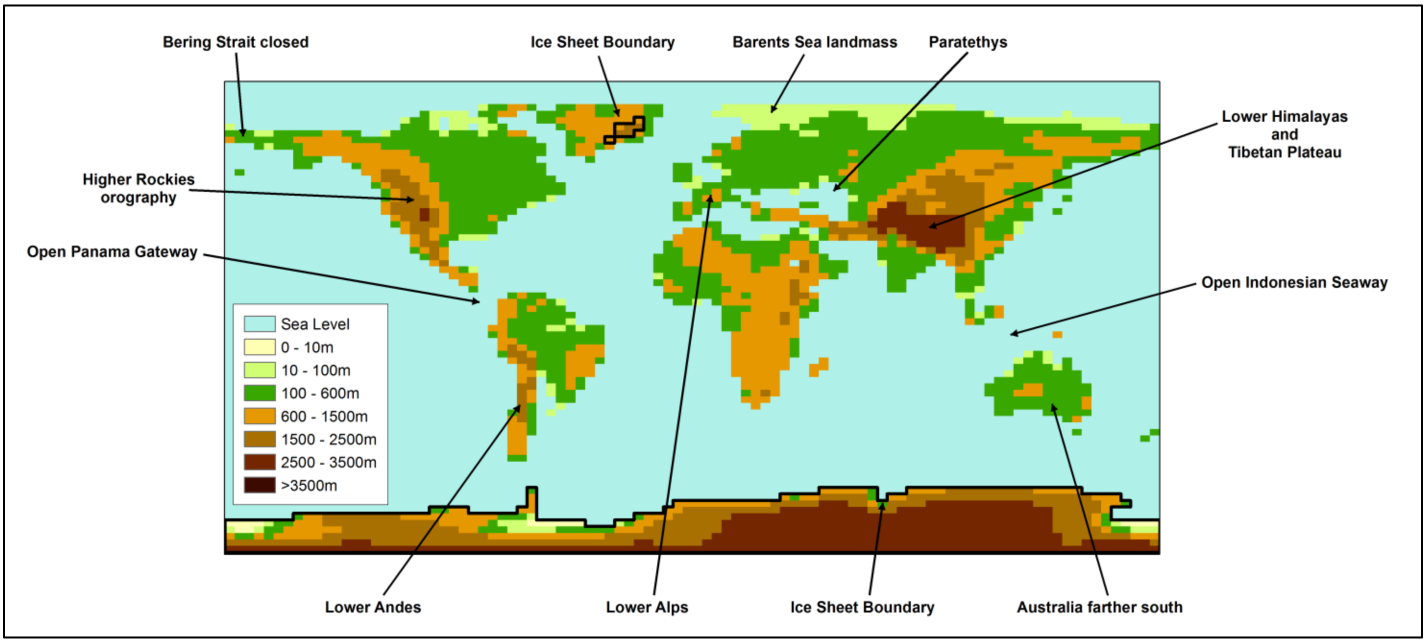

Figure S1. Late Miocene boundary conditions. Bathymetry is unaltered from modern. The colour scale used in this figure groups elevation into bins.

S2.2 Homogenous soils parameters

For the soils parameters that are unknown for the late Miocene, homogenous values have been used as detailed in Table S2. To provide an example of the implications of using these homogenous parameters, the variables thermal capacity and columetric soil moisture concentration at field capacity are shown in Figure S2.

Parameter	Homogenous value
Volumetric soil moisture concentration at wilting point	0.16 m^3/m^3
Volumetric soil moisture concentration atCritical point	0.24 m^3/m^3
Volumetric soil moisture concentration at field capacity	0.24 m^3/m^3
Volumetric soil moisture concentration at saturation	0.46 m^3/m^3
Clapp-Honberger B coefficient	6.6
Thermal conductivity	0.22 J/m/K/s
Saturated soil conductivity	0.005 $kg/m^2/s$
Thermal capacity	$1.2x10^6$ $J/m^3/K$
Saturated soil water suction	0.022 m
Snow-free soil albedo	0.31

Table S2. Homogenous soils parameters

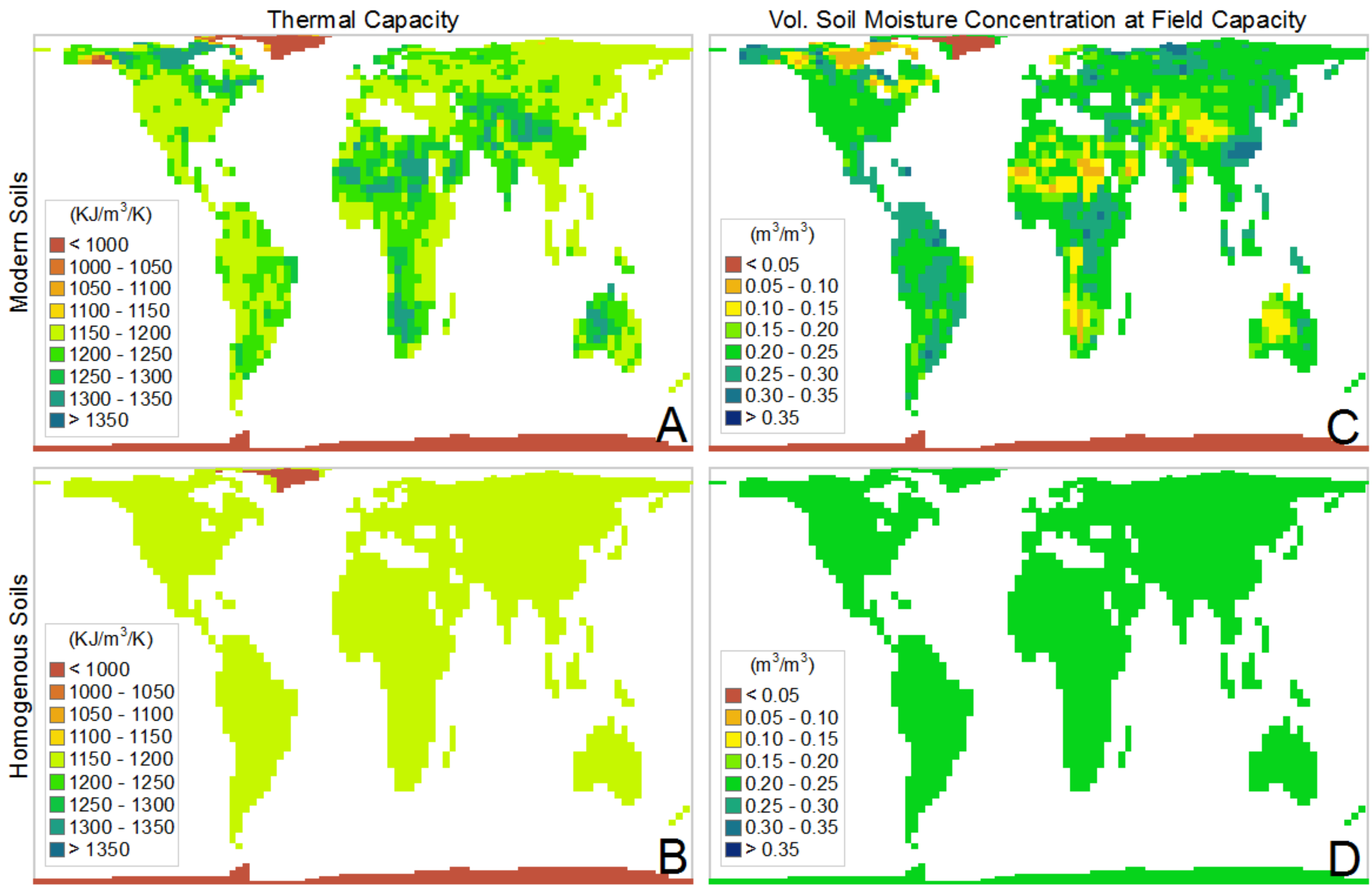

Figure S2. The difference in the parameters for soil thermal capacity and volumetric soil moisture concentration at field capacity used for modern soils and our homogenous assumptions.

S3. Supplementary Results

S3.1 Vegetation distribution sensitivity to soil parameters

The soil sensitivity experiments that were performed for modern boundary conditions show only minor change to the high northern latitude vegetation distributions presented in Sections **Error! Reference source not found.** and **Error! Reference source not found.** when the same uniform soil properties as used for the late Miocene are assumed for the present day (refer to Supplementary Figure S3).

The largest differences in the predicted vegetation occur in the desert regions of Africa, central Asia and north America which reduce in size as compared to the true soil type simulations. The extent of tree cover in Australia and Thailand also reduces when the soil properties are homogenised, being replaced by grasses.

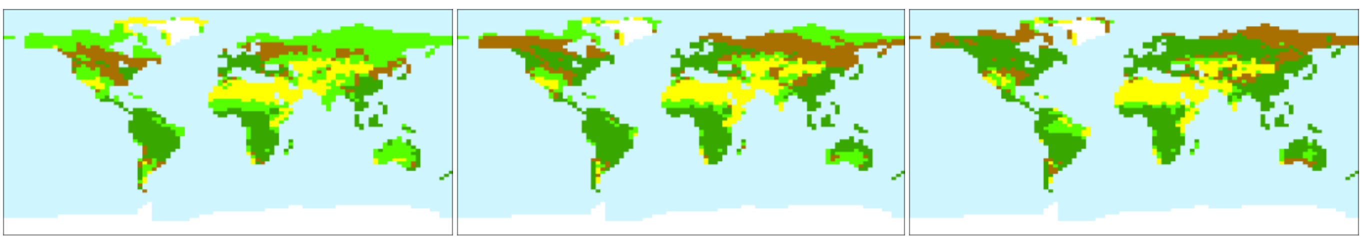

Figure S3. Dominant vegetation distributions for the three CO_2 scenarios: 180ppm, 280ppm and 400ppm as simulated by the TRIFFID vegetation model when homogenous soil parameters are used for the potential modern boundary conditions.

S3.2 Model-data comparison

S3.2.1 Warm Month Mean Temperature (WMT)

The warm month mean temperature is the only variable for which the vegetation changes imposed does not result in any deterioration in the model-data comparison (Figure S4, panel 3). For most of the mid-high latitude data, the best-fit CO_2 scenario is 400 ppm (Figure S5, panels A-C), but the lower latitudes are equally matched with the 400 ppm and the 280 ppm simulation regardless of the vegetation prescribed. There is a similar latitudinal gradient in the best-fit vegetation with the higher latitude data best matching the 400 ppm CO_2 concentration simulation, the mid latitude data best matching the 400 and the 280 ppm simulations and the lowest latitudes being least sensitive to the choice of vegetation, particularly when the CO_2 concentration is highest (Figure S5, panels G-I). Even for the highest CO_2 concentration scenario with the highest CO_2 vegetation distribution the model cannot replicate WMTs as warm as the data reconstructions; only 29% of the datapoints overlap (see Table S5).

S3.2.2 Cold Month Mean Temperature (CMT)

Improvements are seen in the model-data comparison when the vegetation changes from the 180ppm distribution to the 280 ppm distribution (Figure S4, panels A and B) but the number of overlaps between the 400 ppm CO_2 simulations and the data is high for all vegetation distributions (94-95% overlap; Table 6) and so little impact is seen from these vegetation changes (Figure S4, panels C-D). It is notable, given the model-data mismatch for MATs that the southernmost Tortonian datapoints in south-east Asia deteriorate with both vegetation distribution changes. The latitudinal gradient for the best-fit CO_2 concentration is even more defined for the CMT than the WMT; the lower latitudes fit best with the 180ppm simulation and the higher latitudes the 400ppm simulation (Figure S5, panels D-F), and this result is insensitive to the choice of vegetation distribution. However, the best-fit vegetation distribution is very sensitive to the choice of CO_2 concentration - the 180ppm CO_2 concentration requiring the 400ppm vegetation distribution to get close to the temperature reconstructions (Figure S5, panels J-L). The C400V400 simulation results in a model-data overlap of 94% (Table S6).

Stage	Datatype	C180V180	C180V280	C180V400	C280V180	C280V280	C280V400	C400V180	C400V280	C400V400
Messinian	Fauna	3	3	6	6	7	7	7	7	7
	Macroflora	9	10	9	7	7	15	14	26	39
	Microflora	5	5	10	34	40	65	65	90	101
Tortonian	Fauna	8	11	14	14	14	19	19	19	20
	Macroflora	18	20	20	15	14	25	23	39	60
	Microflora	20	20	29	26	27	47	45	57	60
	Total	63	69	88	102	109	178	173	238	287
	% overlap	15	16	21	24	25	41	40	55	67

Table S3. Number of overlaps between the model simulations and the data reconstructions of the mean annual temperature

Stage	Datatype	C180V180	C180V280	C180V400	C280V180	C280V280	C280V400	C400V180	C400V280	C400V400
Messinian	Fauna	136	136	136	136	135	135	135	135	135
	Macroflora	51	51	51	50	50	50	49	49	49
	Microflora	148	148	148	148	147	146	148	146	146
Tortonian	Fauna	506	489	487	483	487	480	482	480	478
	Macroflora	76	76	77	75	75	75	76	74	76
	Microflora	75	77	76	75	76	77	75	75	75
	Total	992	977	975	967	970	963	965	959	959
	% overlap	94	93	93	92	92	92	92	91	91

Table S4. Number of overlaps between the model simulations and the data reconstructions of the mean annual precipitation

Stage	Datatype	C180V180	C180V280	C180V400	C280V180	C280V280	C280V400	C400V180	C400V280	C400V400
Messinian	Fauna	0	0	0	0	0	0	0	0	0
	Macroflora	0	0	0	0	1	4	2	11	13
	Microflora	1	1	3	5	8	10	9	14	14
Tortonian	Fauna	0	0	0	0	0	0	0	0	0
	Macroflora	1	2	2	3	5	9	6	18	24
	Microflora	9	12	14	24	30	37	34	40	45
	Total	11	15	19	32	44	60	51	83	96
	% overlap	3	5	6	10	13	18	15	25	29

Table S5. Number of overlaps between the model simulations and the data reconstructions of the warm month mean temperature

Stage	Datatype	C180V180	C180V280	C180V400	C280V180	C280V280	C280V400	C400V180	C400V280	C400V400
Messinian	Fauna	0	0	0	0	0	0	0	0	0
	Macroflora	22	28	30	33	37	40	43	44	42
	Microflora	103	106	132	134	135	138	142	140	140
Tortonian	Fauna	0	0	0	0	0	0	0	0	0
	Macroflora	36	42	47	51	55	63	68	68	66
	Microflora	42	46	53	56	59	60	64	63	63
	Total	203	222	262	274	286	301	317	315	311
	% overlap	61	67	79	83	86	91	95	95	94

Table S6. Number of overlaps between the model simulations and the data reconstructions of the cold month mean temperature

The individual results of the model-data comparisons for all of the vegetation-CO_2 perturbation experiments now follow

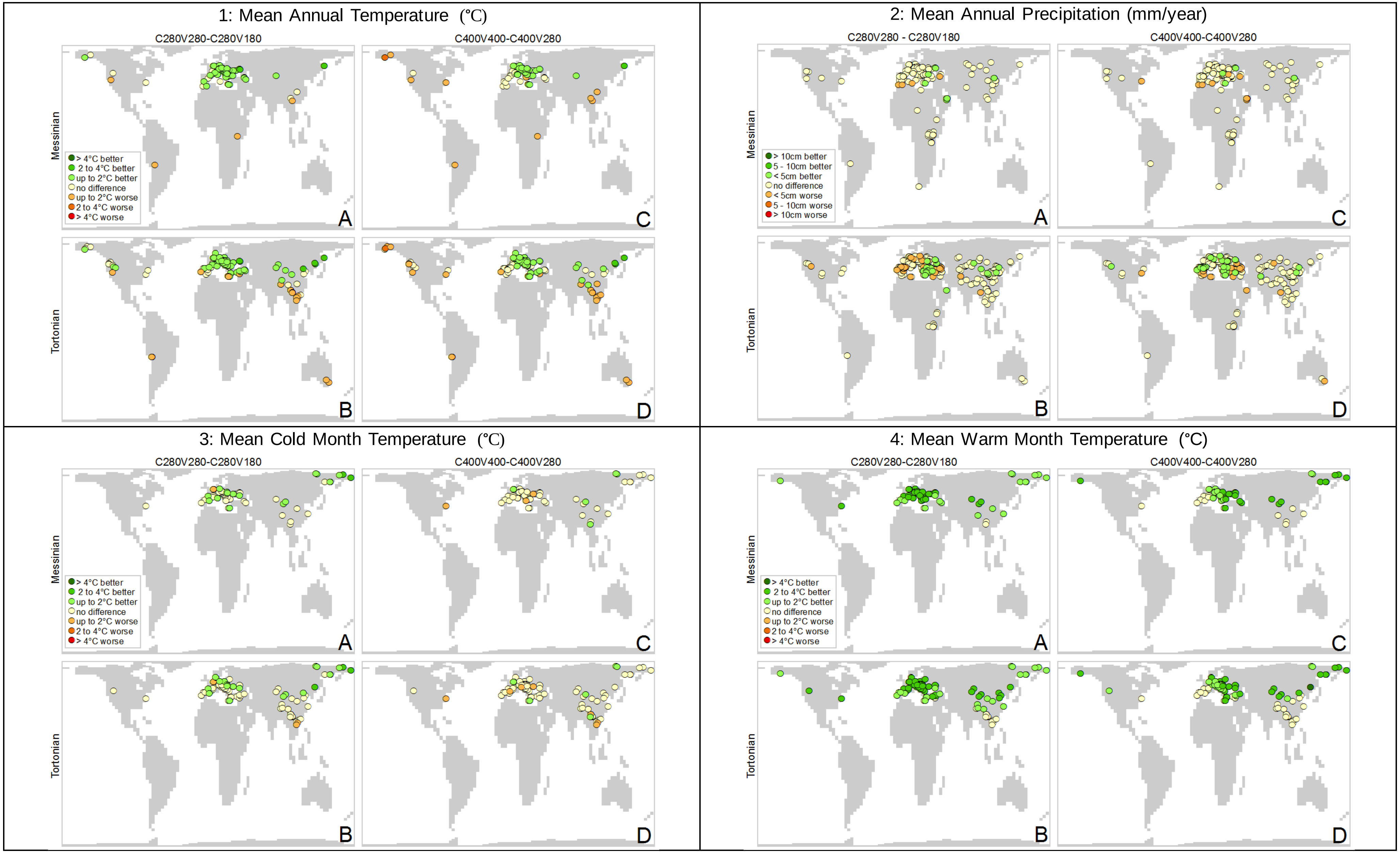

Figure S4. Improvements in the model-data comparison due to vegetation changes Green circles indicate an improvement, red circles indicate a deterioration. The datapoints showing 'no difference' are plotted underneath the other datapoints in order to highlight the differences.

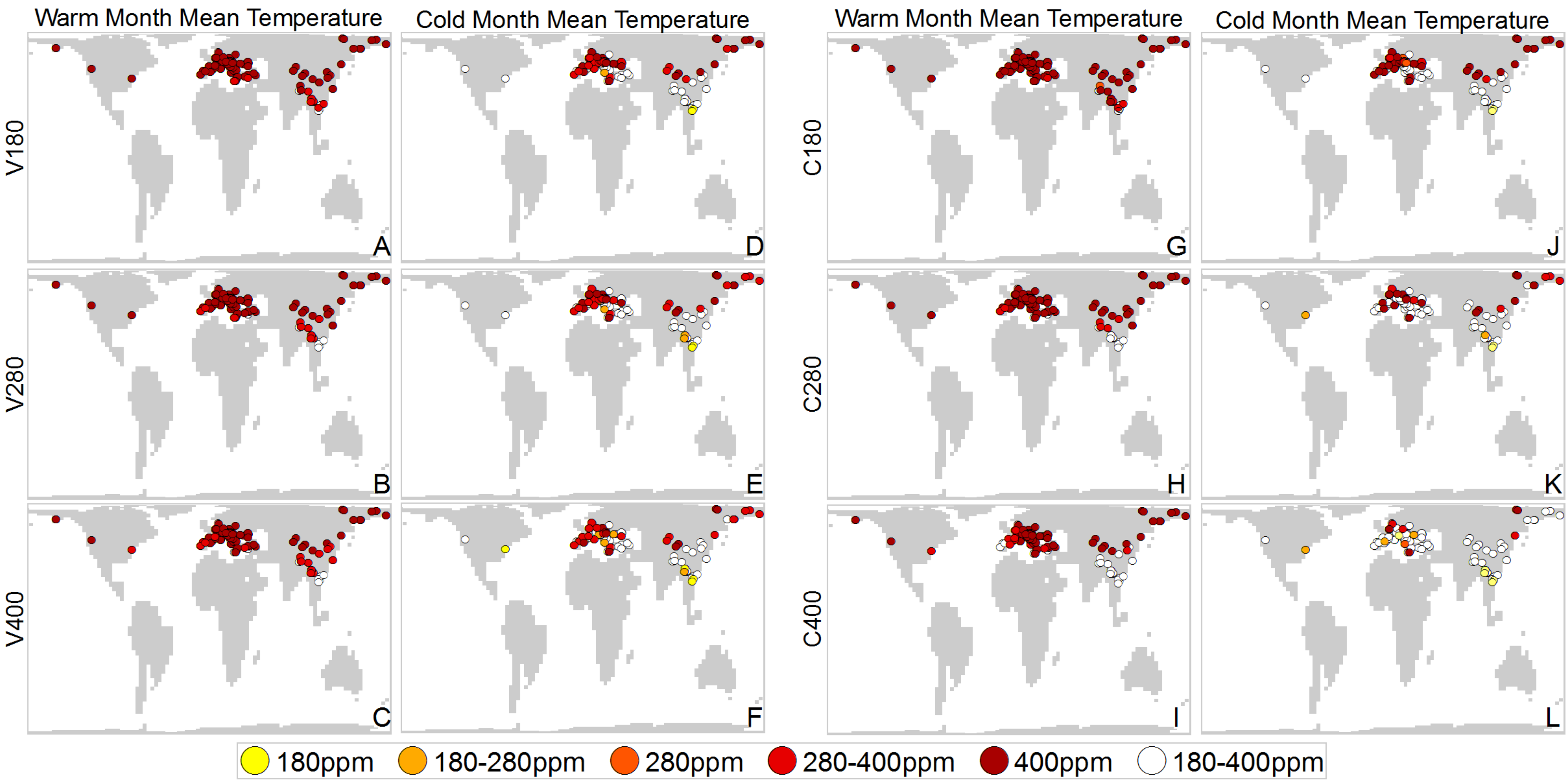

Figure S5. The best-fit scenarios to the data. For the top row, A and D (G and J) show which CO_2 scenario (vegetation) scenario is closest to the data reconstructions when the vegetation distribution (CO_2) imposed is 180ppm. The middle row, B and E (H and K) show which CO_2 (vegetation) scenario is closest to the data reconstructions when the vegetation (CO_2) imposed is 280ppm. The bottom row C and F (I and L) show which CO_2 (vegetation) scenario is closest to the data reconstructions when the vegetation (CO_2) imposed is 400ppm. The datapoints for which there is no discernible difference in the model-data comparison between all of the CO_2 scenarios (i.e. they all overlap with the data) are shown in white and are plotted underneath the other datapoints in order to highlight the differences.

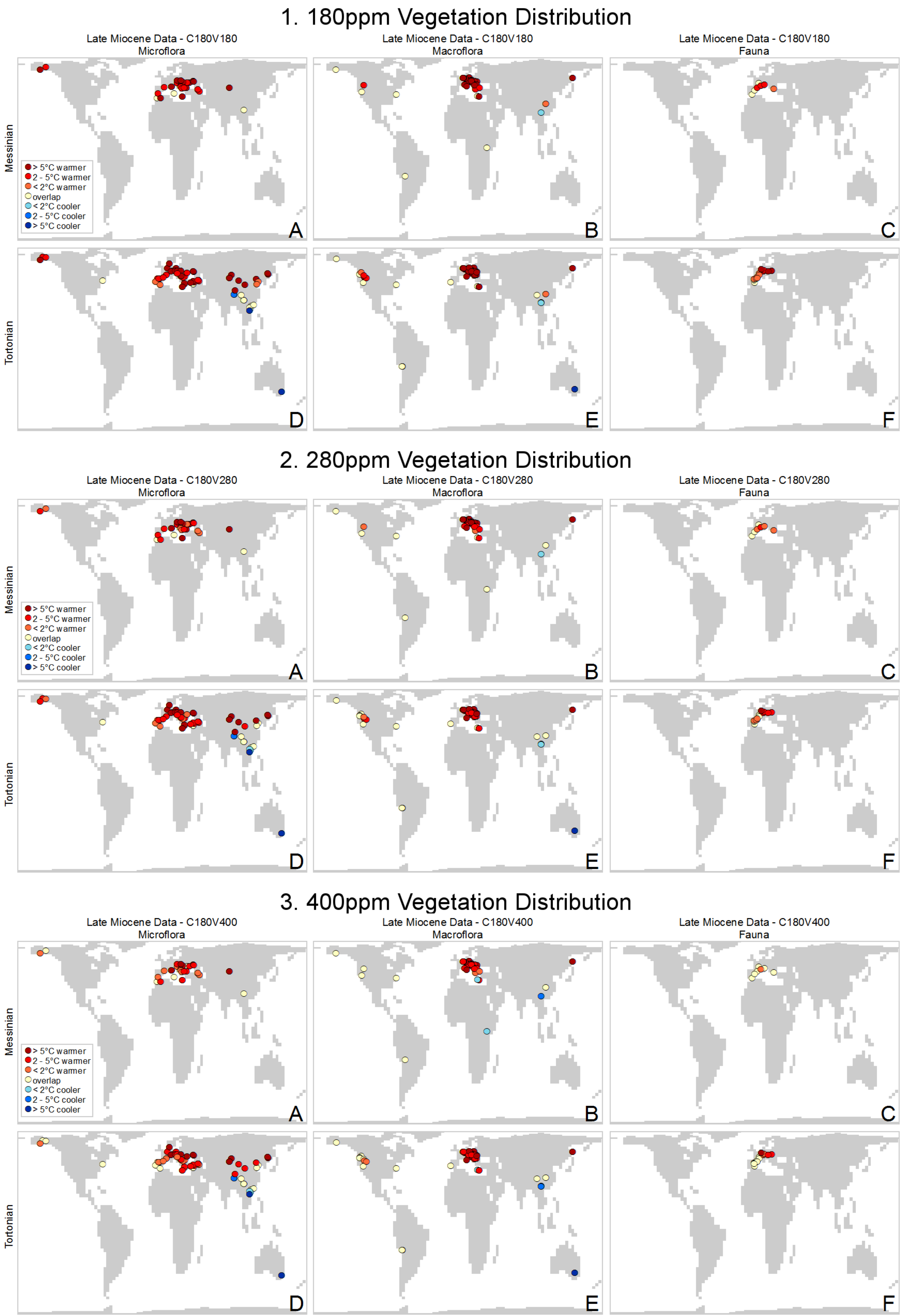

Figure S6. Results from the model-data comparison for mean annual temperature, late Miocene data – 180ppm CO_2 scenarios.

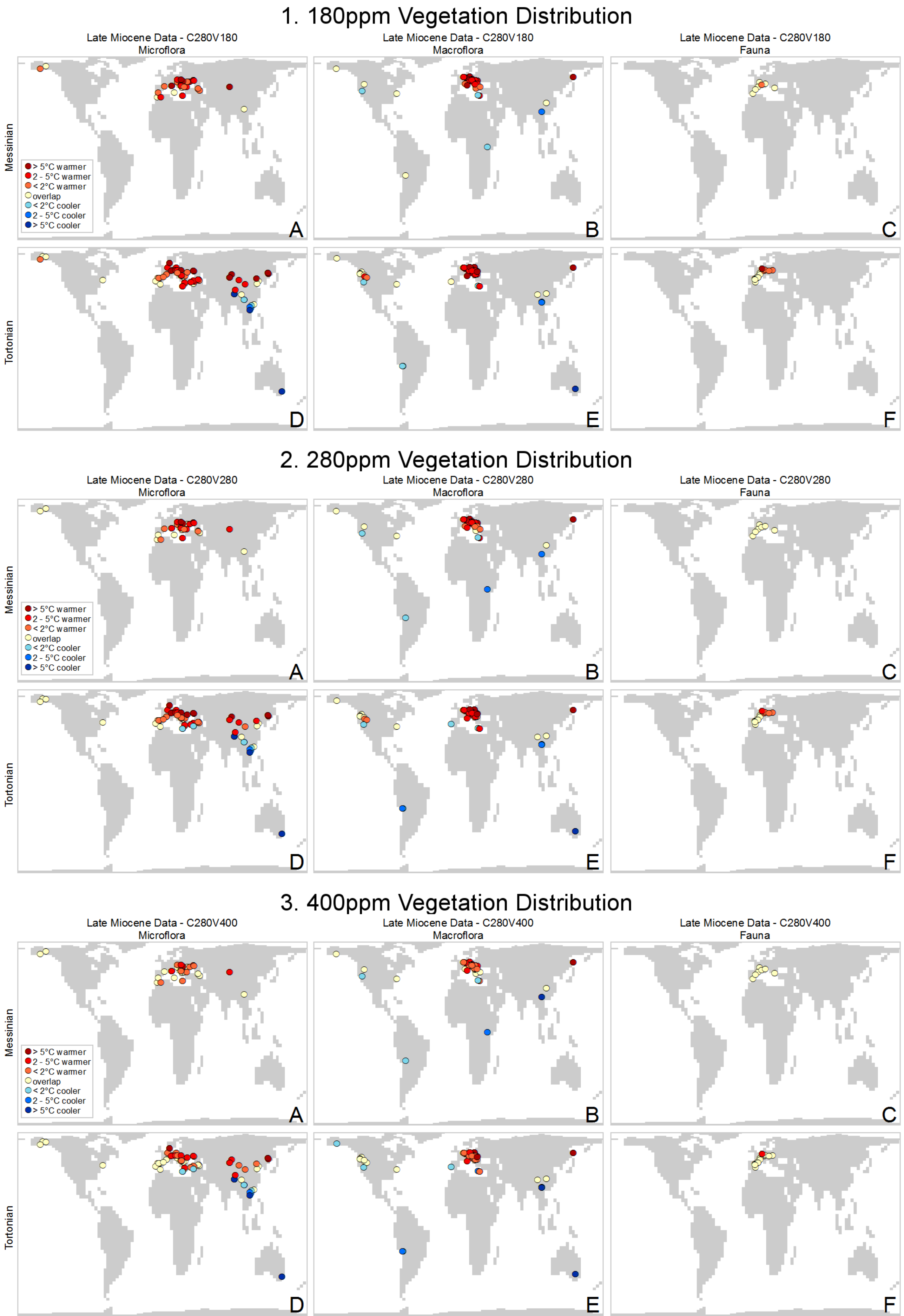

Figure S7. Results from the model-data comparison for mean annual temperature, late Miocene data – 280ppm CO_2 scenarios.

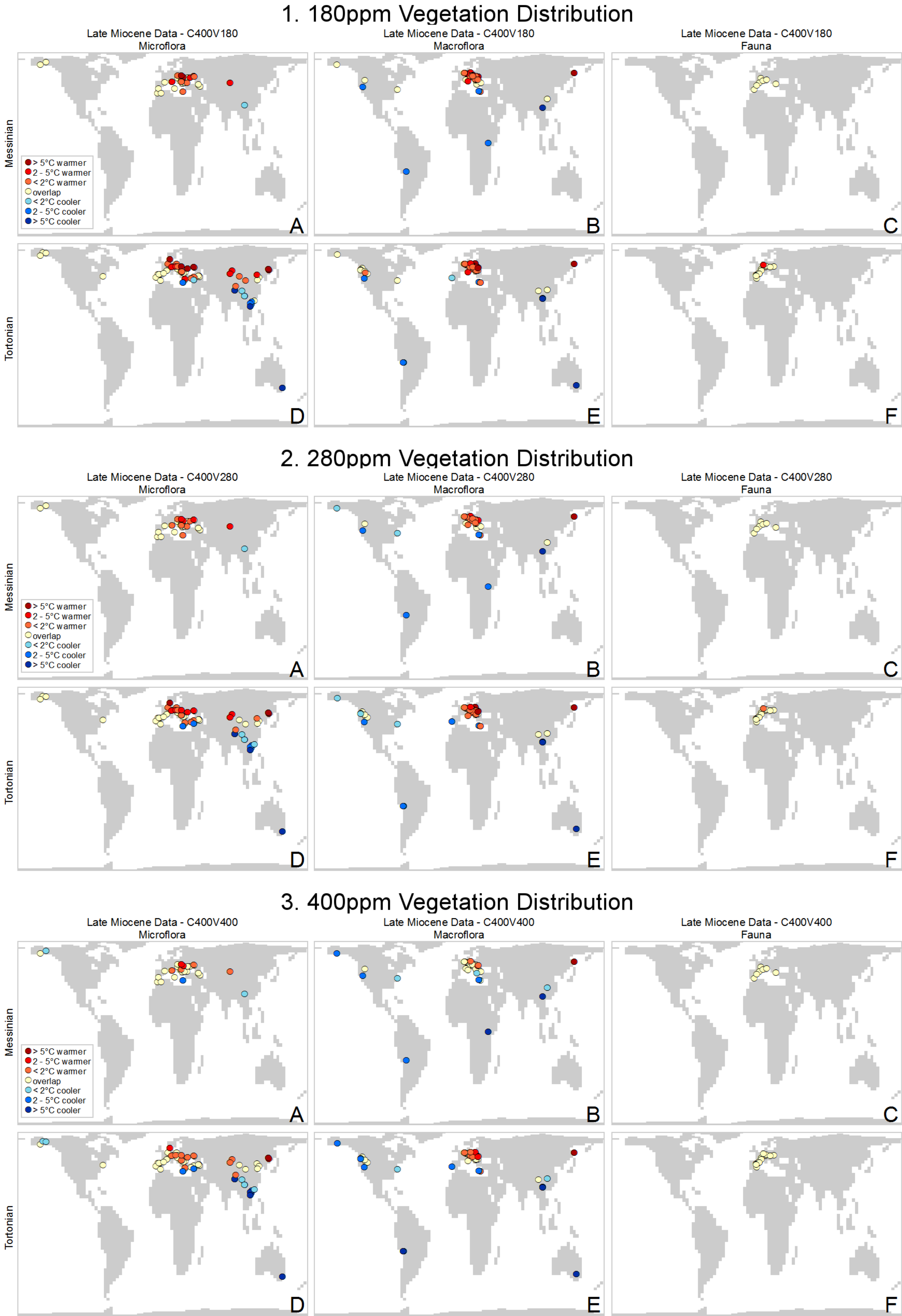

Figure S8. Results from the model-data comparison for mean annual temperature, late Miocene data – 400ppm CO_2 scenarios.

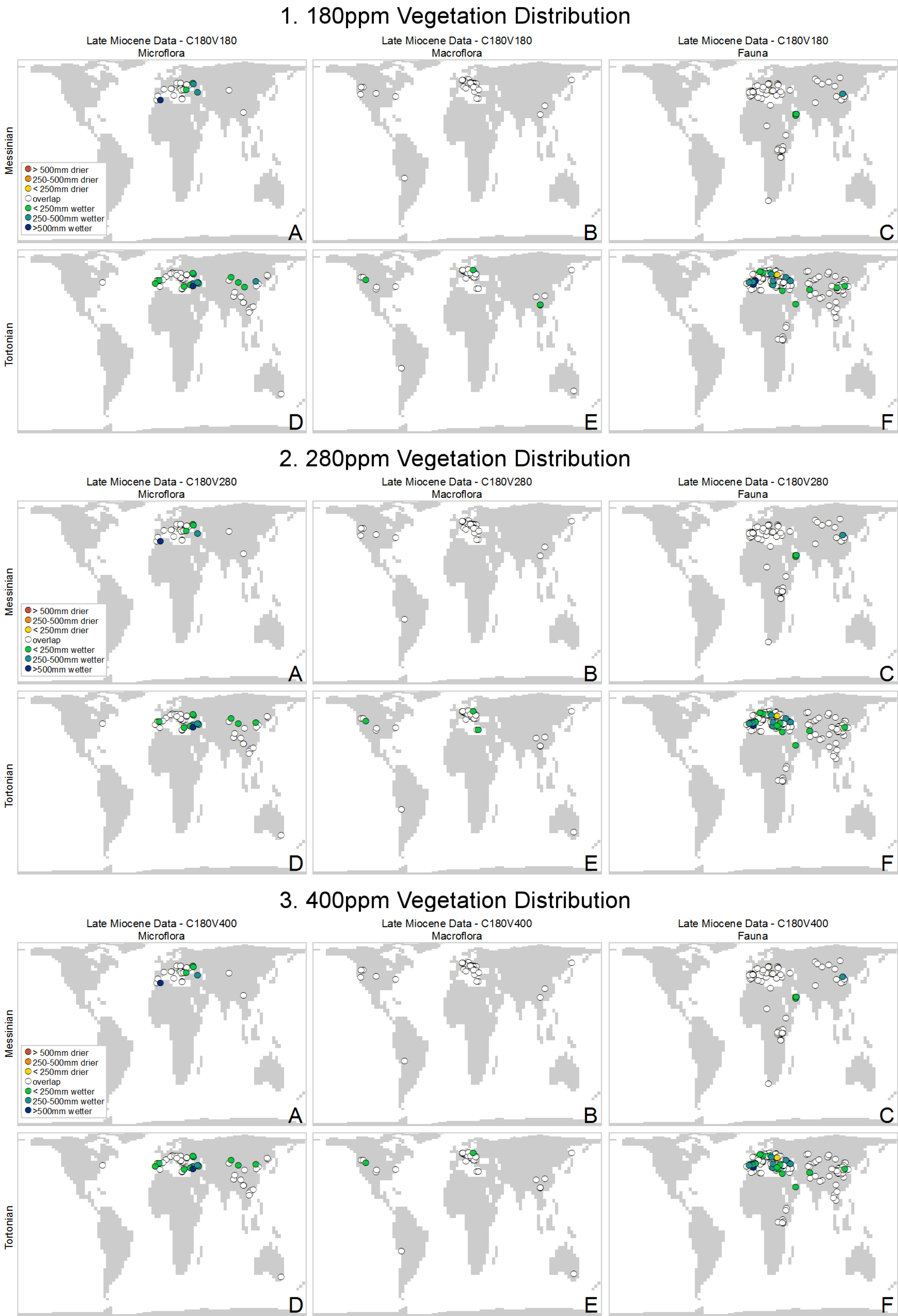

Figure S9. Results from the model-data comparison for mean annual precipitation, late Miocene data – 180ppm CO_2 scenarios.

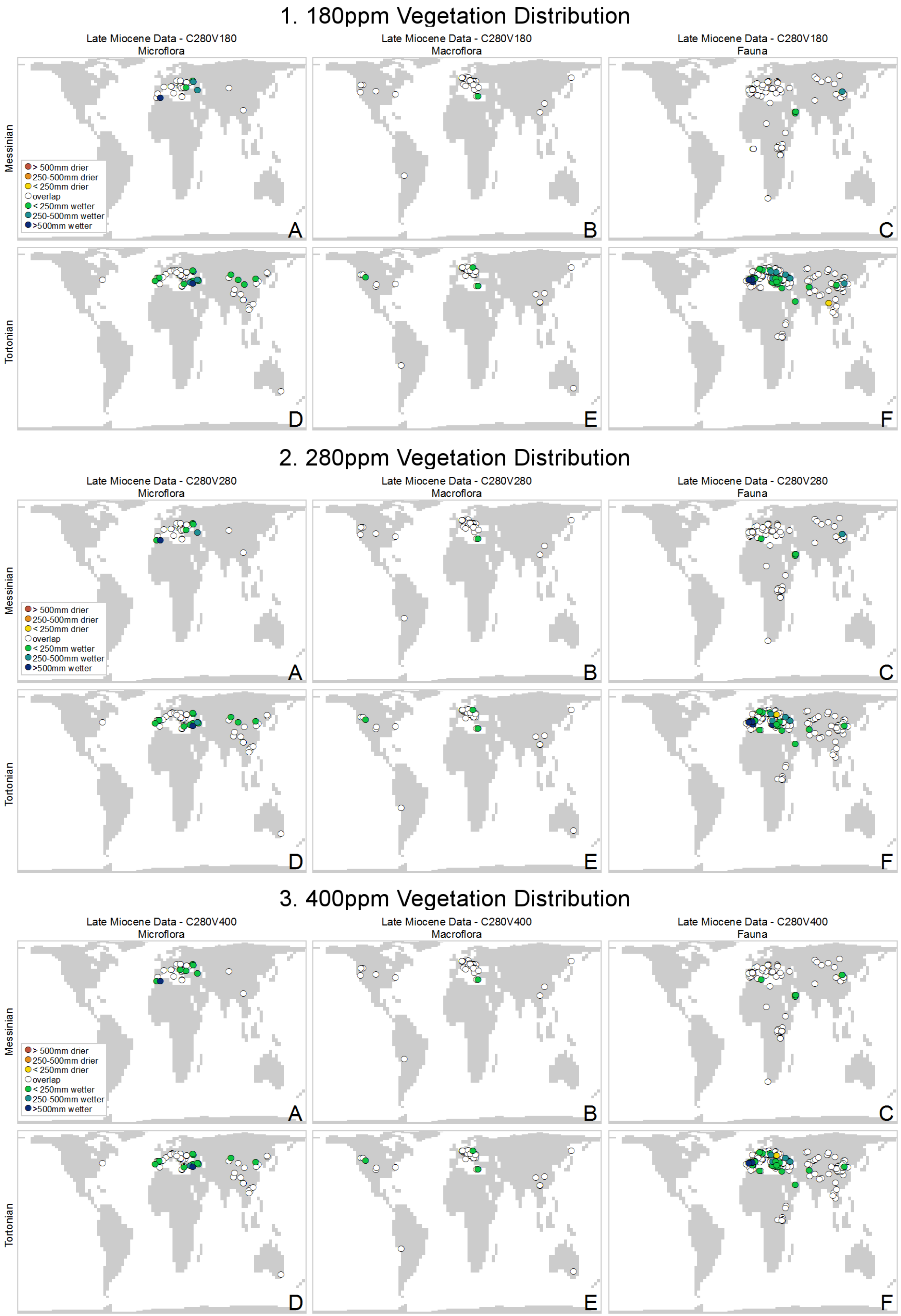

Figure S10. Results from the model-data comparison for mean annual precipitation, late Miocene data – 280ppm CO_2 scenarios.

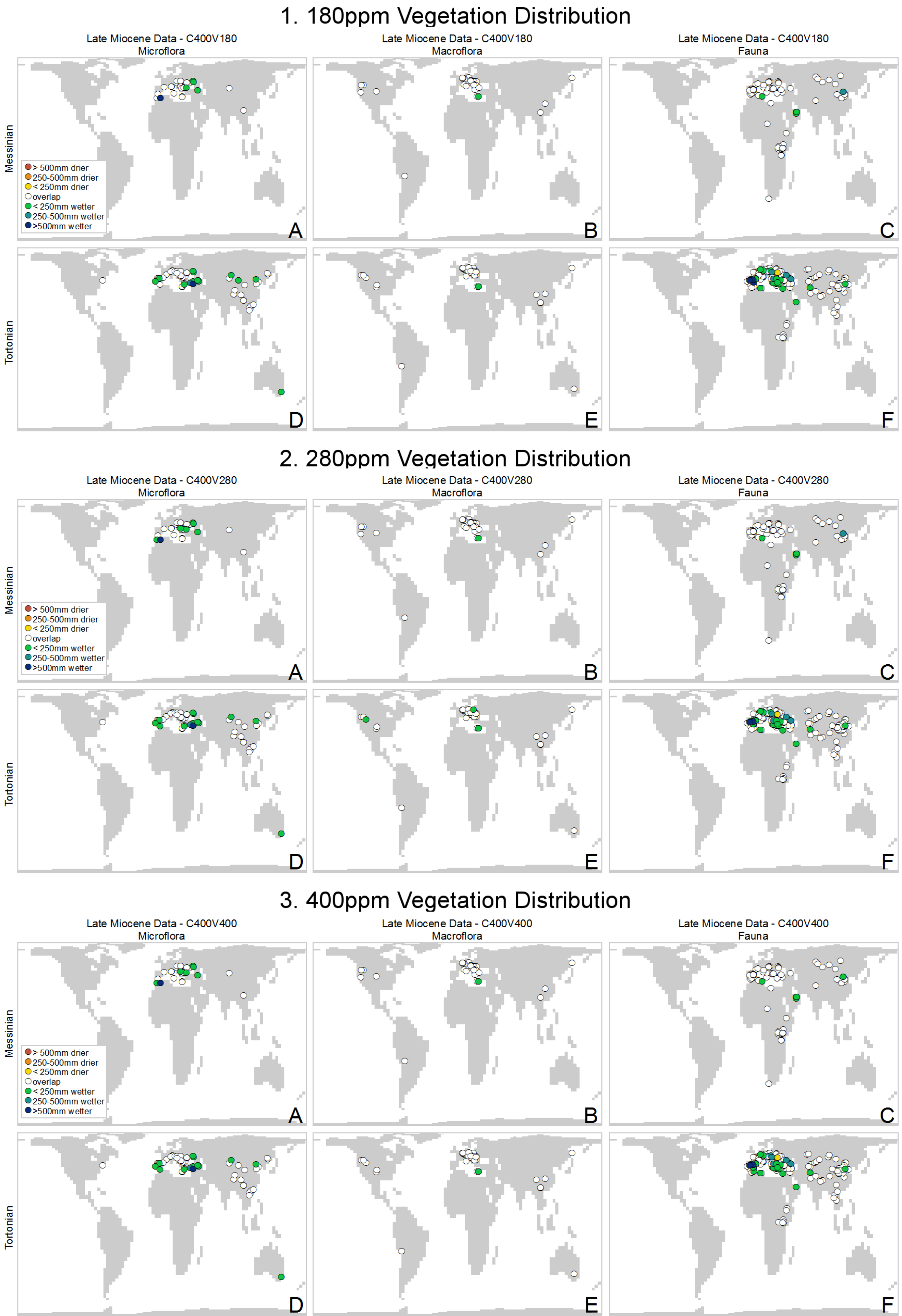

Figure S11. Results from the model-data comparison for mean annual precipitation, late Miocene data – 400ppm CO_2 scenarios.

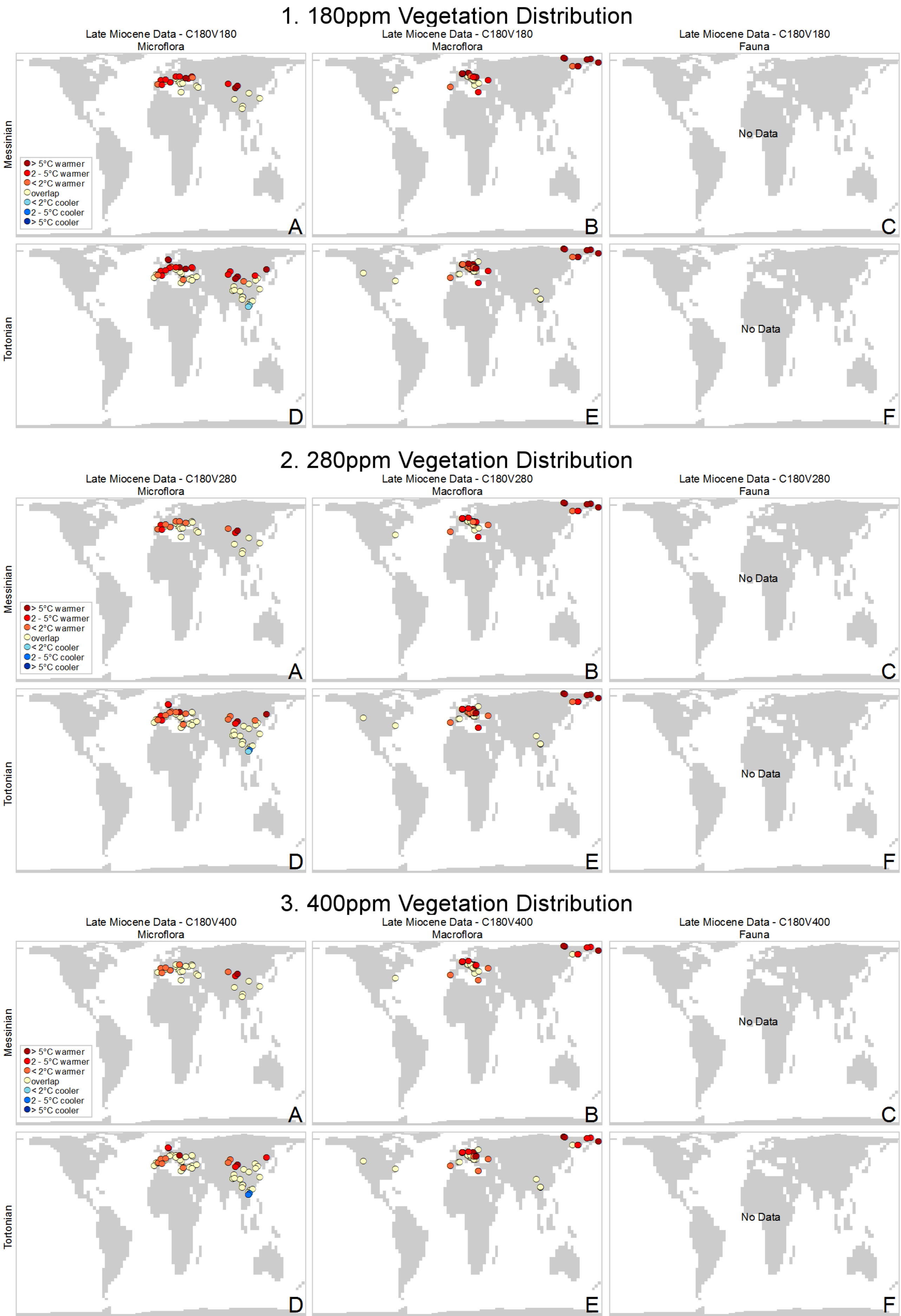

Figure S12. Results from the model-data comparison for the coldest month mean temperature, late Miocene data – 180ppm CO_2 scenarios.

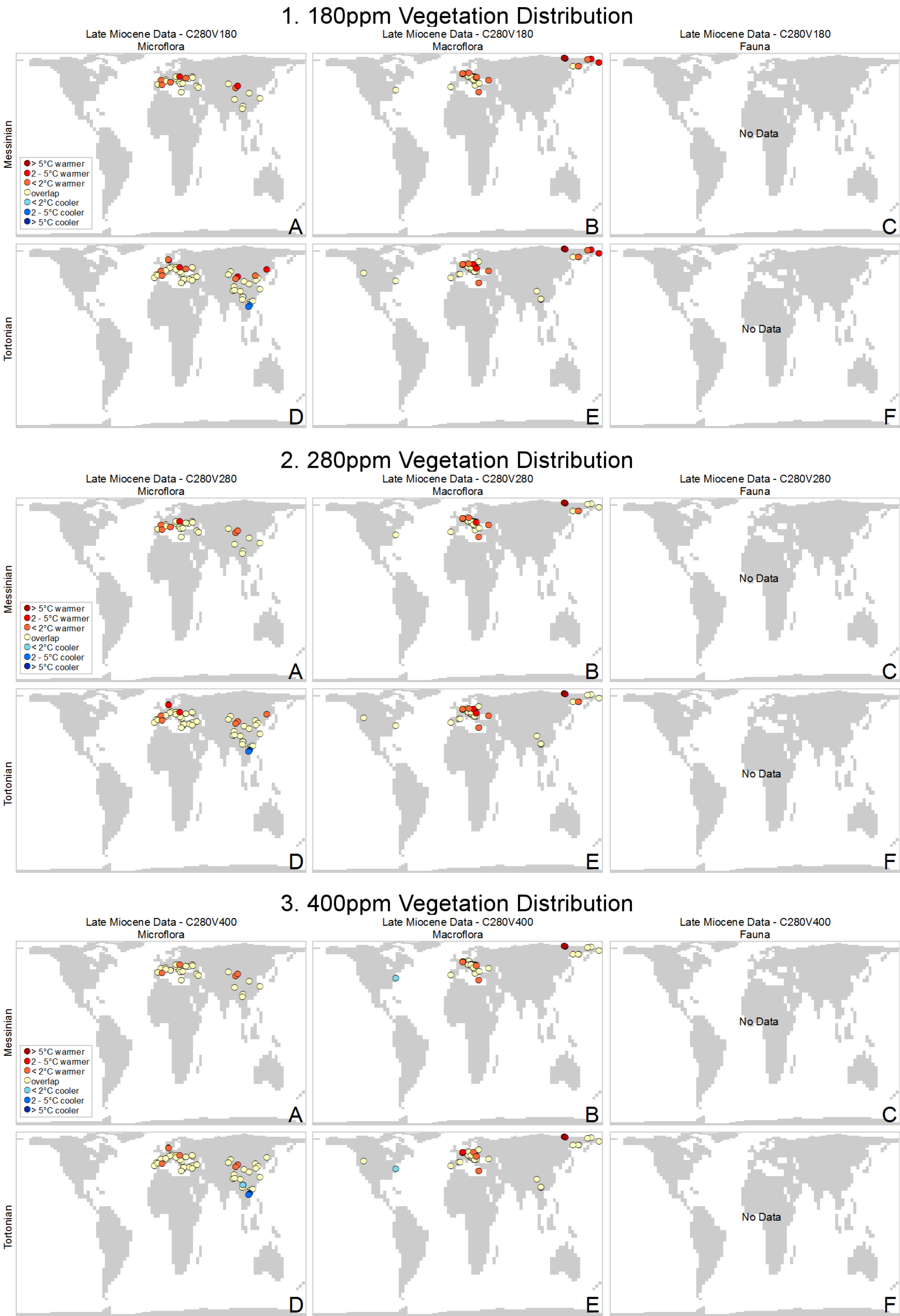

Figure S13. Results from the model-data comparison for the coldest month mean temperature, late Miocene data – 280ppm CO_2 scenarios.

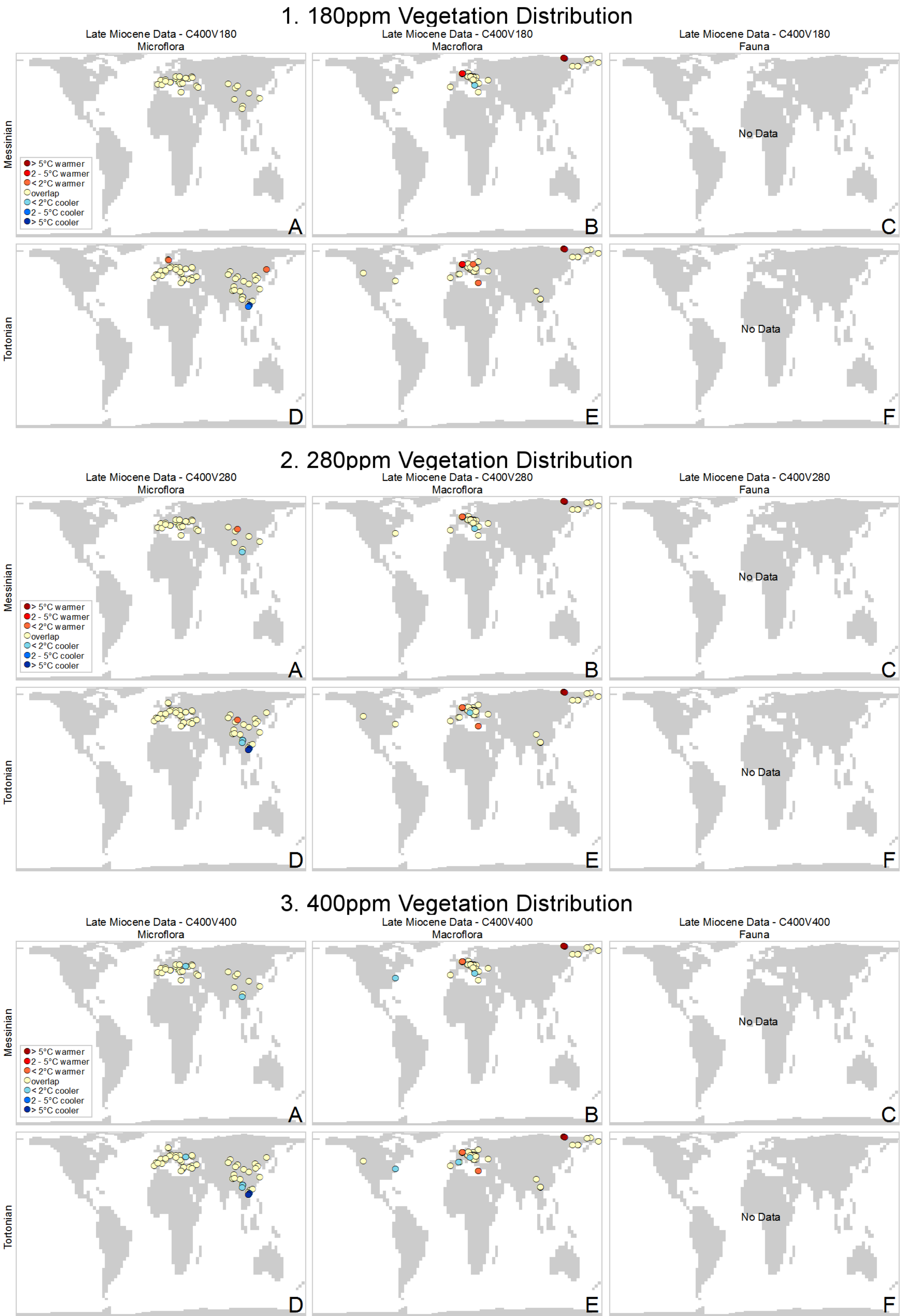

Figure S14. Results from the model-data comparison for the coldest month mean temperature, late Miocene data – 400ppm CO_2 scenarios.

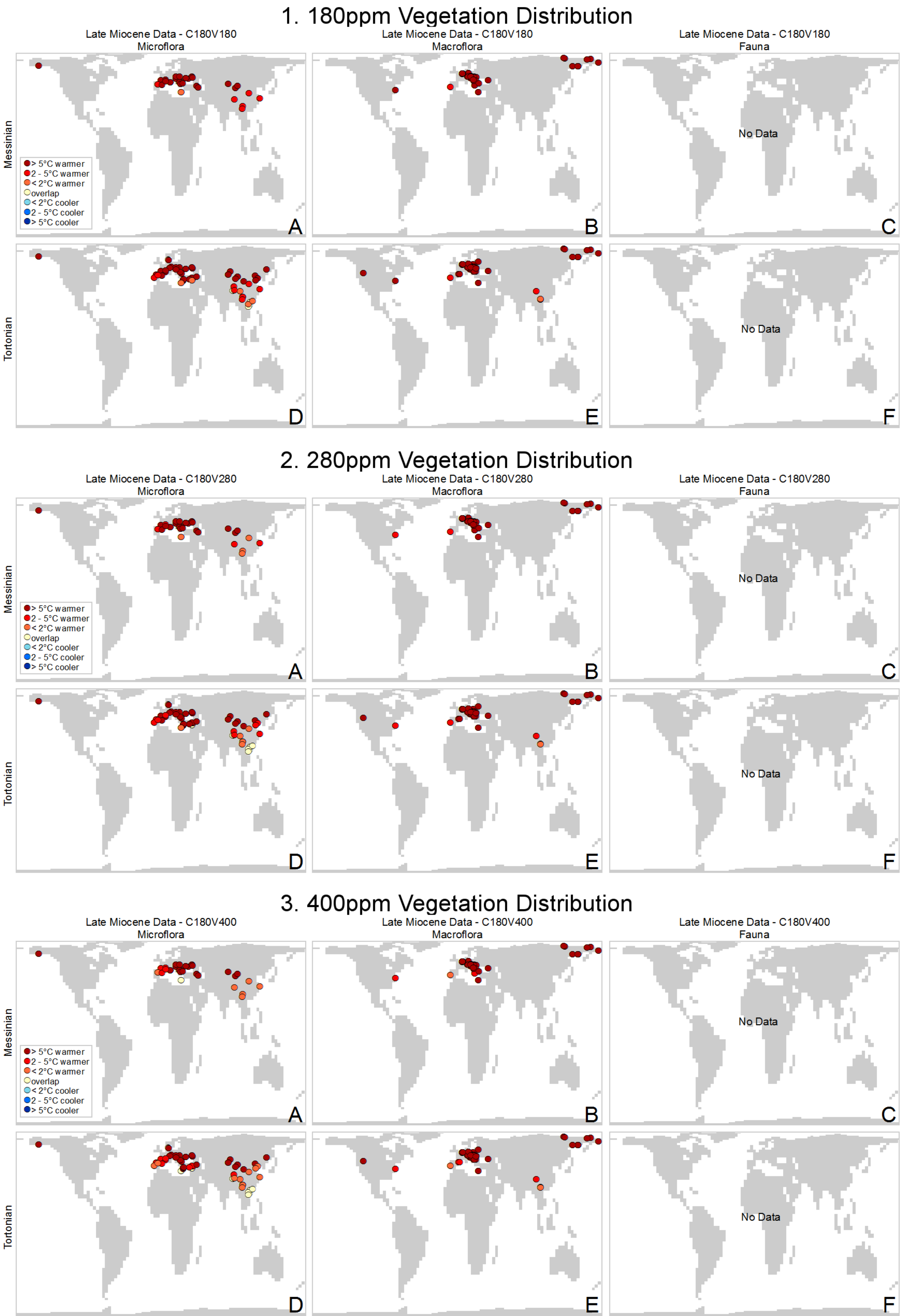

Figure S15. Results from the model-data comparison for the warmest month mean temperature, late Miocene data – 180ppm CO_2 scenarios.

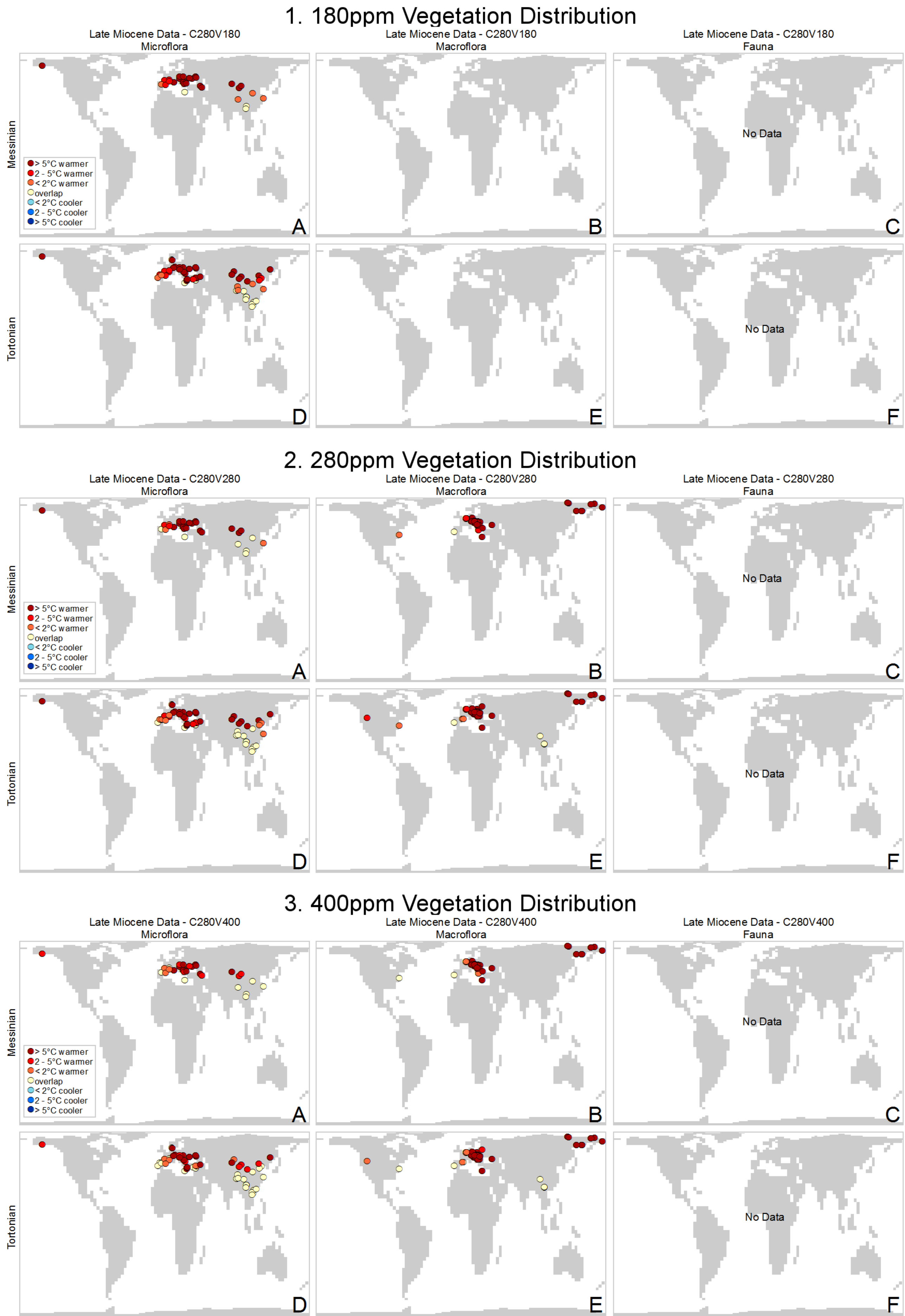

Figure S16. Results from the model-data comparison for the warmest month mean temperature, late Miocene data – 280ppm CO_2 scenarios.

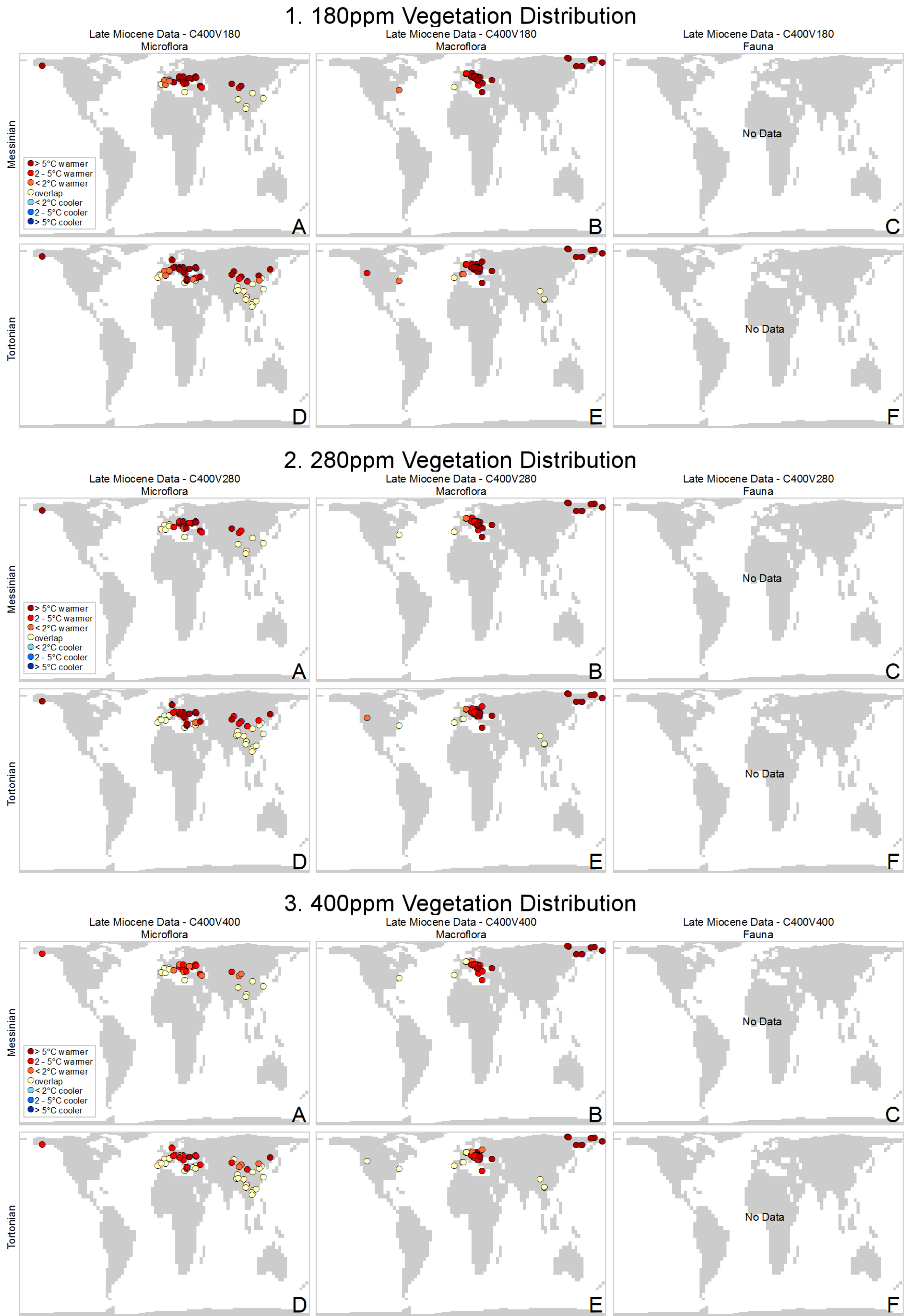

Figure S17. Results from the model-data comparison for the warmest month mean temperature, late Miocene data – 400ppm CO_2 scenarios

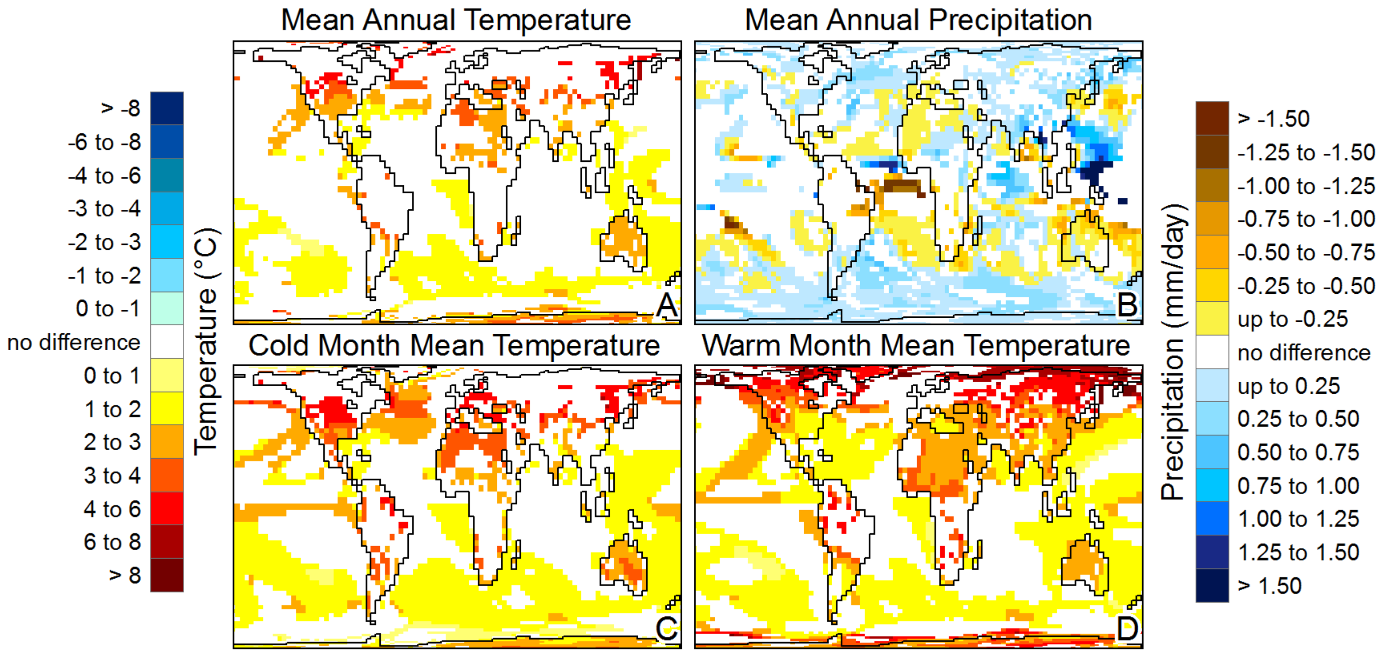

Figure S18. Regions where late Miocene palaeodata could be used to inform potential future climate changes.

S4. References

Betts, R.A., Cox, P.M., Collins, M., Harris, P.P., Huntingford, C., Jones, C.D., 2004. The role of ecosystem-atmosphere interactions in simulated Amazonian precipitation decrease and forest dieback under global climate warming. Theoretical and Applied Climatology 78, 157-175.

Cane, M.A., Molnar, P., 2001. Closing of the Indonesian seaway as a precursor to east African aridircation around 3-4 million years ago. Nature 411, 157-162.

Cox, P., Huntingford, C., Harding, R., 1998. A canopy conductance and photosynthesis model for use in a GCM land surface scheme. J Hydrol 212, 79-94.

Duque-Caro, H., 1990. NEOGENE STRATIGRAPHY, PALEOCEANOGRAPHY AND PALEOBIOGEOGRAPHY IN NORTHWEST SOUTH-AMERICA AND THE EVOLUTION OF THE PANAMA SEAWAY. Palaeogeography Palaeoclimatology Palaeoecology 77, 203-234.

Edwards, A.R., 1975. Southwest Pacific Cenozoic paleogeography and an integrated Neogene paleocirculation model. Init. Rep. DSDP 30, 667–684.

Fang, X.M., Yan, M.D., Van der Voo, R., Rea, D.K., Song, C.H., Pares, J.M., Gao, J.P., Nie, J.S., Dai, S., 2005. Late Cenozoic deformation and uplift of the NE Tibetan plateau: Evidence from high-resolution magneto stratigraphy of the Guide Basin, Qinghai Province, China. Geological Society of America Bulletin 117, 1208-1225.

Garzione, C.N., Hoke, G.D., Libarkin, J.C., Withers, S., MacFadden, B., Eiler, J., Ghosh, P., Mulch, A., 2008. Rise of the Andes. Science 320, 1304-1307.

Gladenkov, A.Y., Oleinik, A.E., Marincovich Jr, L., Barinov, K.B., 2002. A refined age for the earliest opening of Bering Strait. Palaeogeography, Palaeoclimatology, Palaeoecology 183, 321-328.

Gregory-Wodzicki, K.M., 2002. A late Miocene subtropical-dry flora from the northern Altiplano, Bolivia. Palaeogeography Palaeoclimatology Palaeoecology 180, 331-348.

Harrison, T.M., Copeland, P., Kidd, W.S.F., Yin, A., 1992. Raising Tibet. Science 255, 1663-1670.

Henderson-Sellers, A., 1993. Continental vegetation as a dynamic component of a global climate model: a preliminary assessment. Climatic Change 23, 337-377.

Hughes, J.K., Valdes, P.J., Betts, R.A., 2006. Dynamics of a global-scale vegetation model. Ecological Modelling 198, 452-462.

Keigwin, L., 1982. Isotopic paleoceanography of the Caribbean and East Pacific: role of Panama uplift in late Neogene time. Science 217, 350-353.

Kennett, J.P., Keller, G., Srinivasan, M.S., 1985. Miocene Planktonic Foraminiferal Biogeography and Paleoceanographic Development of the Indo-Pacific Region. Geol Soc Am Mem 163, 197-236.

Kuhlemann, J., 2007. Paleogeographic and paleotopographic evolution of the Swiss and Eastern Alps since the Oligocene. Global Planet Change 58, 224-236.

Loveland, T.R., Belward, A.S., 1997. The IGBP-DIS Global 1 km Land Cover Data Set, DISCover First Results. International Journal of Remote Sensing 18, 3,289-283,295.

Marincovich Jr, L., Gladenkov, A.Y., 2001. New evidence for the age of Bering Strait. Quaternary Sci Rev 20, 329-335.

Marincovich, L., Gladenkov, A.Y., 1999. Evidence for an early opening of the Bering Strait. Nature 397, 149-151.

Molnar, P., England, P., Martinod, J., 1993. Mantle Dynamics, Uplift of the Tibetan Plateau, and the Indian Monsoon. Rev Geophys 31, 357-396.

Morgan, P., Swanberg, C.A., 1985. On the Cenozoic Uplift and Tectonic Stability of the Colorado Plateau. J Geodyn 3, 39-63.

Rowley, D.B., Currie, B.S., 2006. Palaeo-altimetry of the late Eocene to Miocene Lunpola basin, central Tibet. Nature 439, 677-681.

Saggerson, E.P., Baker, B.H., 1965. Post-Jurassic erosion-surfaces in eastern Kenya and their deformation in relation to rift structure. Quarterly Journal of the Geological Society of London 121, 51-72.

Spiegel, C., Kuhlemann, J., Dunkl, I., Frisch, W., 2001. Paleogeography and catchment evolution in a mobile orogenic belt: the Central Alps in Oligo-Miocene times. Tectonophysics 341, 33-47.

Svenning, J.-C., Skov, F., 2004. Limited filling of the potential range in European tree species. Ecol Lett 7, 565-573.

Svirezhev, Y., 2000. Lotka-volterra models and the global vegetation pattern. Ecological Modelling 135, 135-146.

van Andel, T.H., Heath, G.R., Moore, T.C., Jr., 1975. Cenozoic history and paleoceanography of the Central Equatorial Pacific Ocean. Geological Society of America Memoir 143, 134p.

Woodward, F.I., Lomas, M.R., Betts, R.A., 1998. Vegetation–climate feedbacks in a greenhouse world. philosophical Transaction of the Royal Society B 353, 29-39.

Yemane, K., Bonnefille, R., Faure, H., 1985. Paleoclimatic and Tectonic Implications of Neogene Microflora from the Northwestern Ethiopian Highlands. Nature 318, 653-656.

CO_2 Change	Period	Variable	$C180_{TRIF}$	$C280_{TRIF}$	C280V180	C180V280	f_{CO2}	f_{VEG}	f_{SYN}
180 to 280ppm	Late Miocene	Temperature (°C)	10.1	13.2	12.6	10.9	2.4	0.7	-0.2
		Precipitation (mm/yr)	986	1043	1033	1000	45	12	-3.3
	Potential Modern	Temperature (°C)	10.1	12.9	12.2	11.1	1.9	0.8	-0.3
		Precipitation (mm/yr)	987	1040	1024	1007	35	18	-4.0

CO_2 Change	Period	Variable	$C280_{TRIF}$	$C400_{TRIF}$	C400V280	C280V400	f_{CO2}	f_{VEG}	f_{SYN}
280 to 400ppm	Late Miocene	Temperature (°C)	13.2	15.8	15.0	14.0	1.8	0.8	-0.1
		Precipitation (mm/yr)	1043	1082	1072	1055	28	11	-0.9
	Potential Modern	Temperature (°C)	12.9	15.2	14.7	13.8	1.6	0.7	-0.5
		Precipitation (mm/yr)	1040	1077	1066	1054	25	13	-3.4

	Climate Sensitivity (°C)		
2 x CO_2	*Late Miocene*	*Modern*	*Late Miocene – Modern*
from 180ppm	4.85	4.31(4.25)	0.54(0.6)
from 280ppm	5.01	4.43(4.21)	0.55(0.8)

	2 x CO_2	*Climate Sensitivity (°C)*	
		Late Miocene	*Potential Modern*
Incl. vegetation changes	*from 180ppm*	4.85	4.31
Excl. vegetation changes		3.61	3.60
Change due to vegetation		1.24	0.71
Incl. vegetation changes	*from 280ppm*	5.01	4.43
Excl. vegetation changes		3.62	4.03
Change due to vegetation		1.39	0.40

Abbreviation	Meaning
LM	Late Miocene boundary conditions
PM	Potential Modern boundary conditions
BF	Fractional coverage of broadleaf forest
NF	Fractional coverage of needleleaf forest
C3	Fractional coverage of C3 grasses
C4	Fractional coverage of C4 grasses
SB	Fractional coverage of shrubs
BS	Fractional coverage of bare soil
SAT	Near-surface air temperature (deg C)
PRE	Precipitation (mm/day)
-9999	Missing data

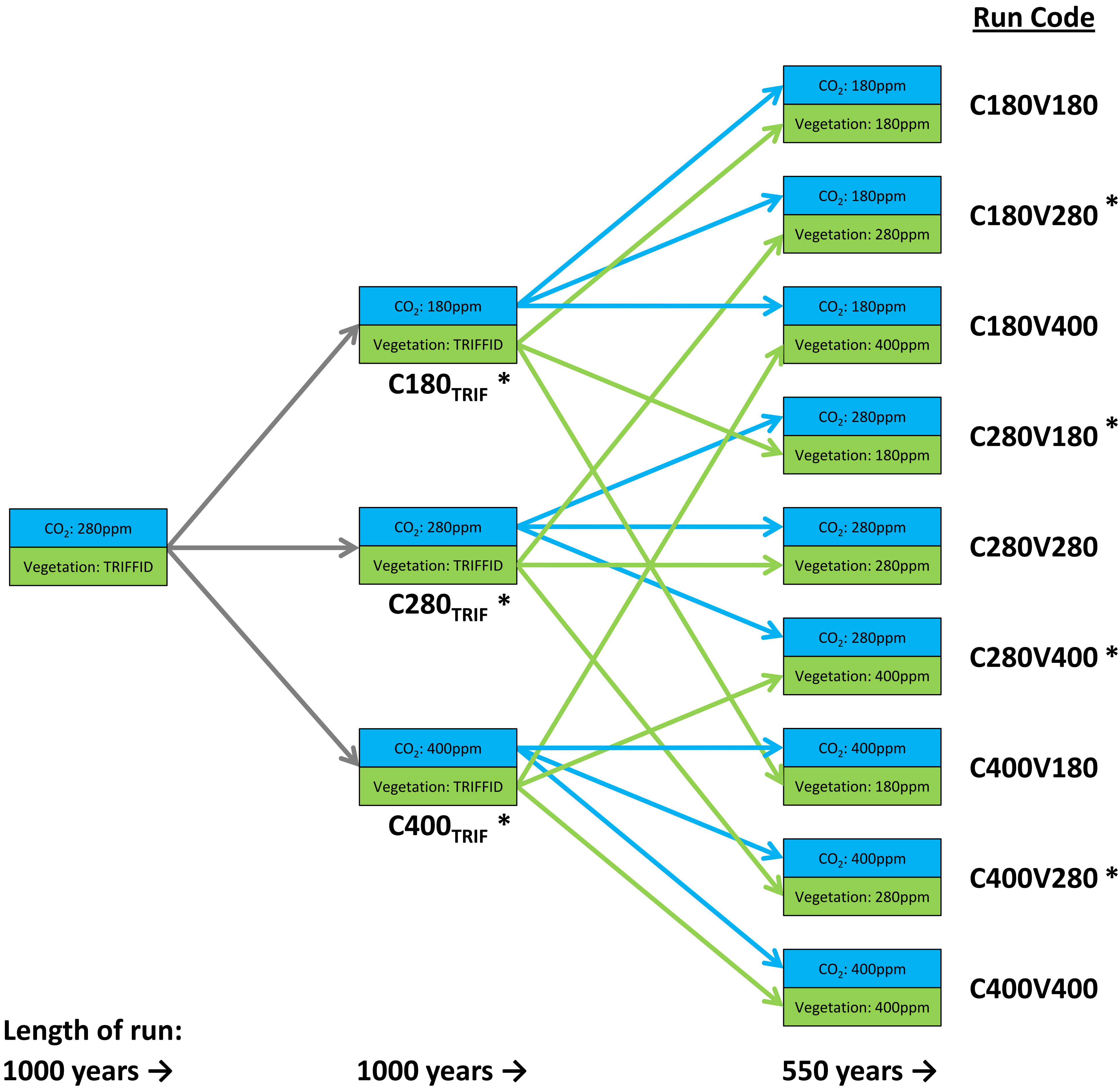

Run Code
CO2: 280ppm
Vegetation: TRIFFID
CO2: 180ppm
Vegetation: TRIFFID
C180TRIF *
CO2: 280ppm
Vegetation: TRIFFID
C280TRIF *
CO2: 400ppm
Vegetation: TRIFFID
C400TRIF *
CO2: 180ppm
Vegetation: 180ppm
C180V180
CO2: 180ppm
Vegetation: 280ppm
C180V280 *
CO2: 180ppm
Vegetation: 400ppm
C180V400
CO2: 280ppm
Vegetation: 180ppm
C280V180 *
CO2: 280ppm
Vegetation: 280ppm
C280V280
CO2: 280ppm
Vegetation: 400ppm
C280V400 *
CO2: 400ppm
Vegetation: 180ppm
C400V180
CO2: 400ppm
Vegetation: 280ppm
C400V280 *
CO2: 400ppm
Vegetation: 400ppm
C400V400
Length of run:
1000 years →
1000 years →
550 years →

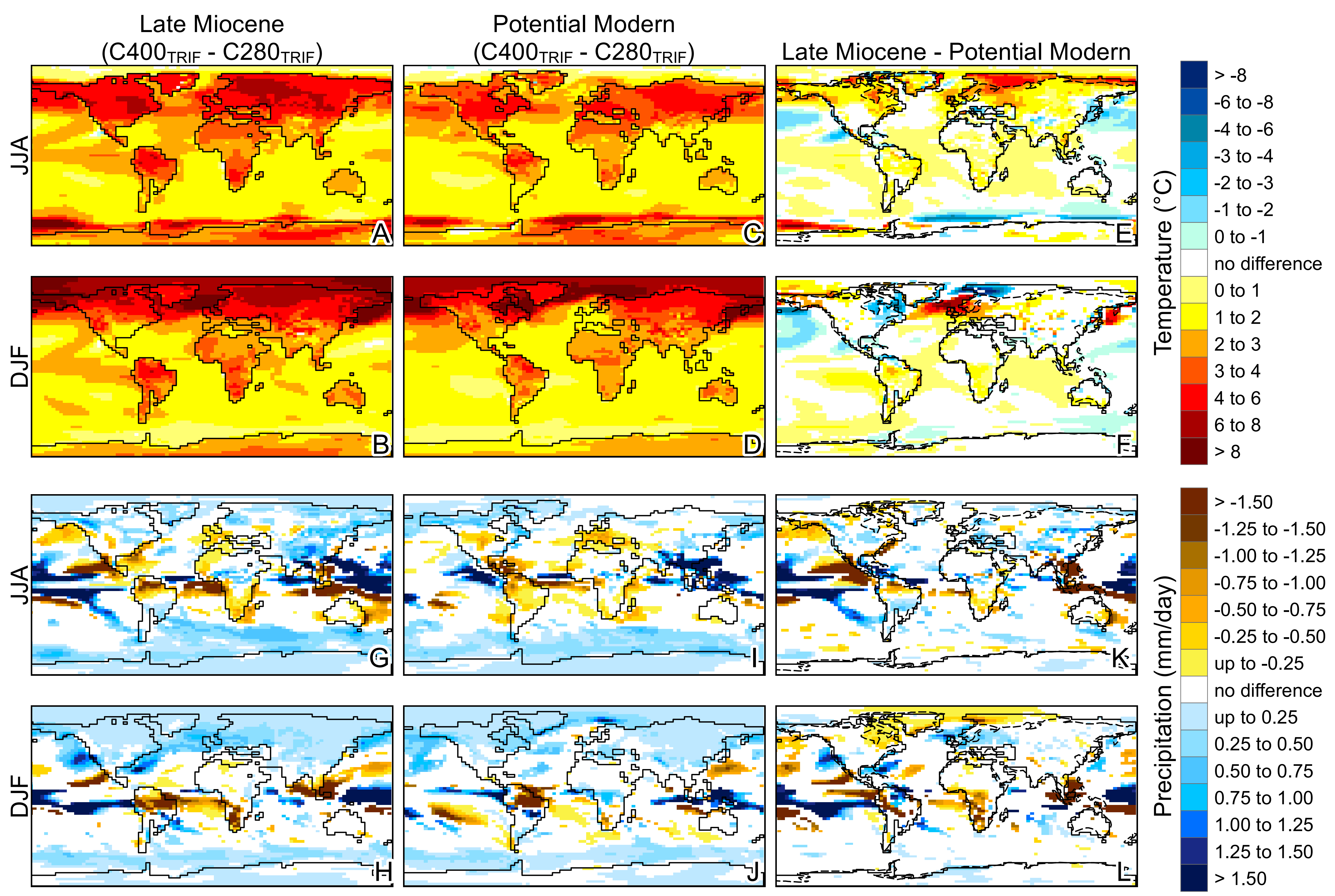

Late Miocene
(C400TRIF - C280TRIF)
Potential Modern
(C400TRIF - C280TRIF)
Late Miocene - Potential Modern
JJA
DJF
JJA
DJF
A
B
C
D
E
F
G
H
I
J
K
L
Temperature (°C)
> -8
-6 to -8
-4 to -6
-3 to -4
-2 to -3
-1 to -2
0 to -1
no difference
0 to 1
1 to 2
2 to 3
3 to 4
4 to 6
6 to 8
> 8
Precipitation (mm/day)
> -1.50
-1.25 to -1.50
-1.00 to -1.25
-0.75 to -1.00
-0.50 to -0.75
-0.25 to -0.50
up to -0.25
no difference
up to 0.25
0.25 to 0.50
0.50 to 0.75
0.75 to 1.00
1.00 to 1.25
1.25 to 1.50
> 1.50

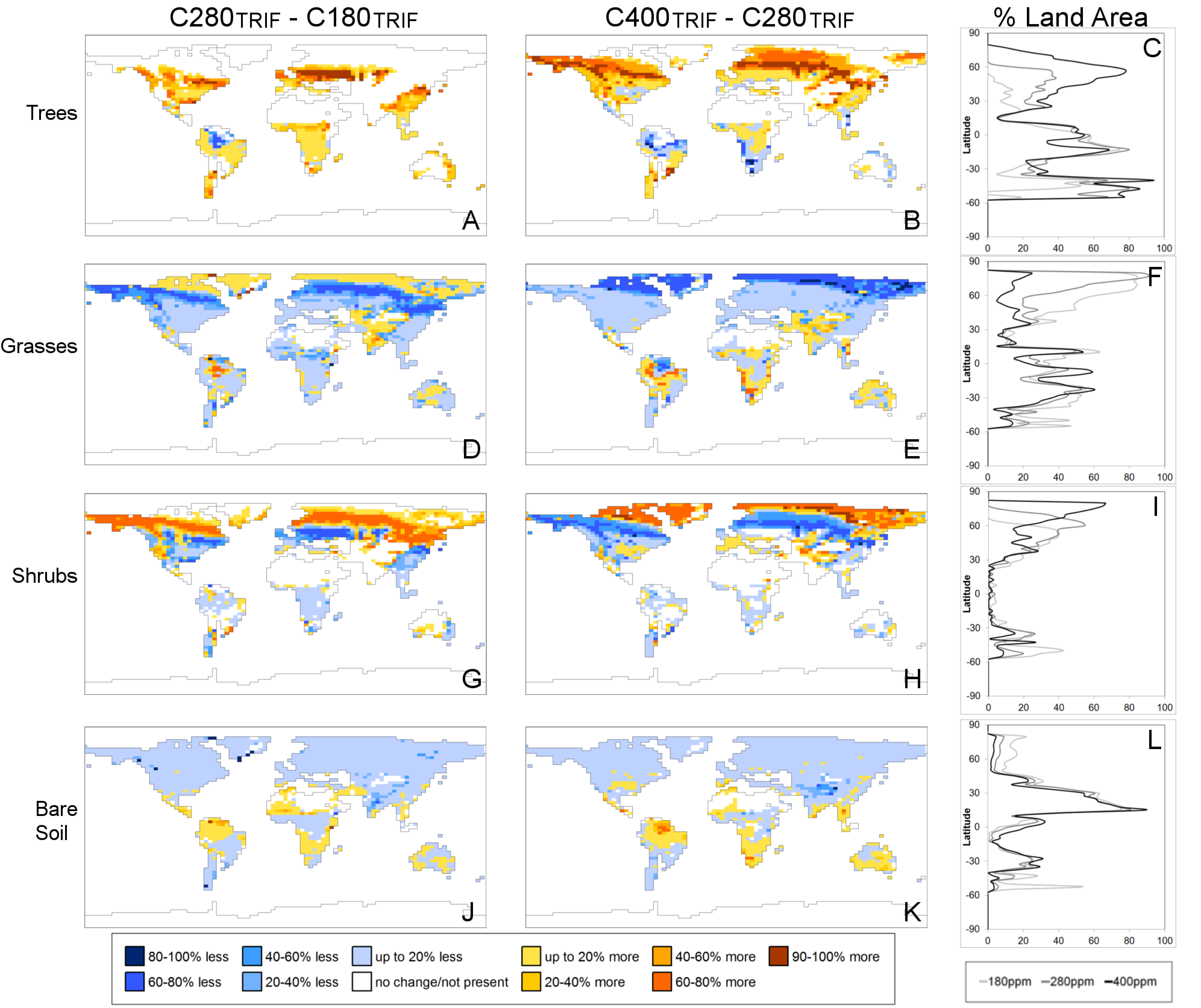

C280TRIF - C180TRIF
C400TRIF - C280TRIF
% Land Area
Trees
Grasses
Shrubs
Bare Soil
A
B
C
D
E
F
G
H
I
J
K
L
Latitude
80-100% less
60-80% less
40-60% less
20-40% less
up to 20% less
no change/not present
up to 20% more
20-40% more
40-60% more
60-80% more
90-100% more
180ppm
280ppm
400ppm

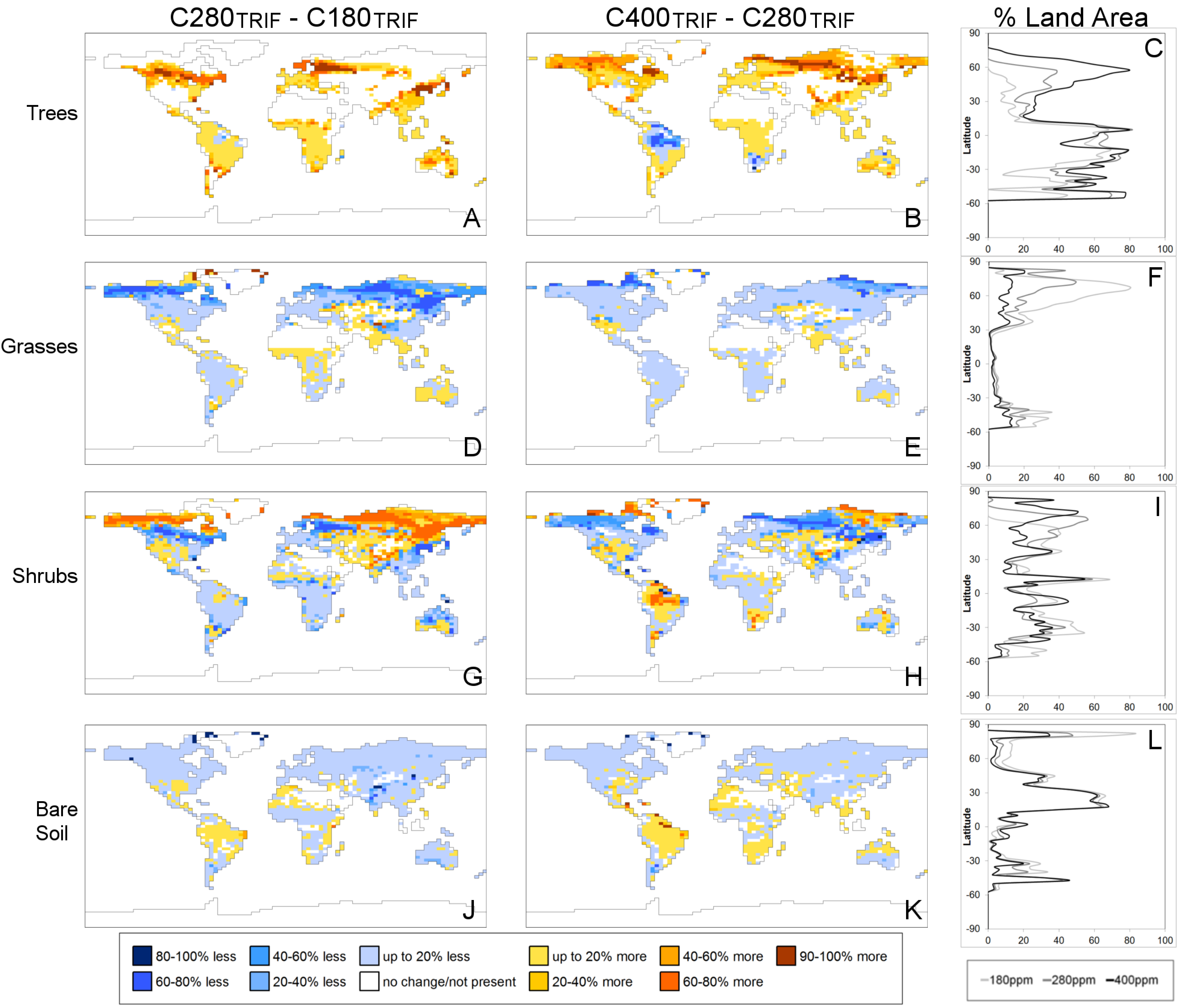

C280TRIF - C180TRIF
C400TRIF - C280TRIF
% Land Area
Trees
Grasses
Shrubs
Bare Soil
A
B
C
D
E
F
G
H
I
J
K
L
Latitude
80-100% less
60-80% less
40-60% less
20-40% less
up to 20% less
no change/not present
up to 20% more
20-40% more
40-60% more
60-80% more
90-100% more
180ppm
280ppm
400ppm

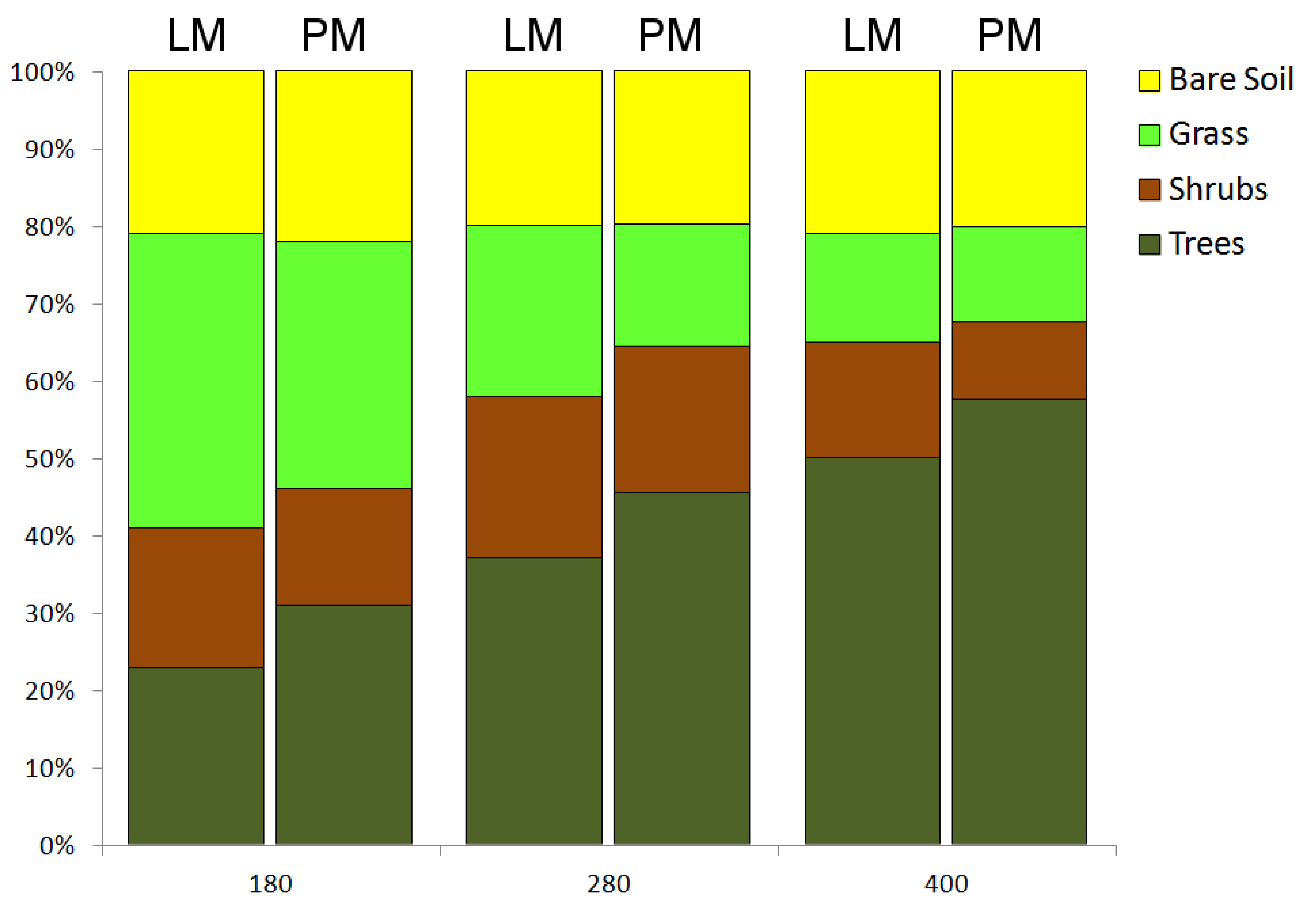
LM
PM
LM
PM
LM
PM
100%
90%
80%
70%
60%
50%
40%
30%
20%
10%
0%
180
280
400
Bare Soil
Grass
Shrubs
Trees

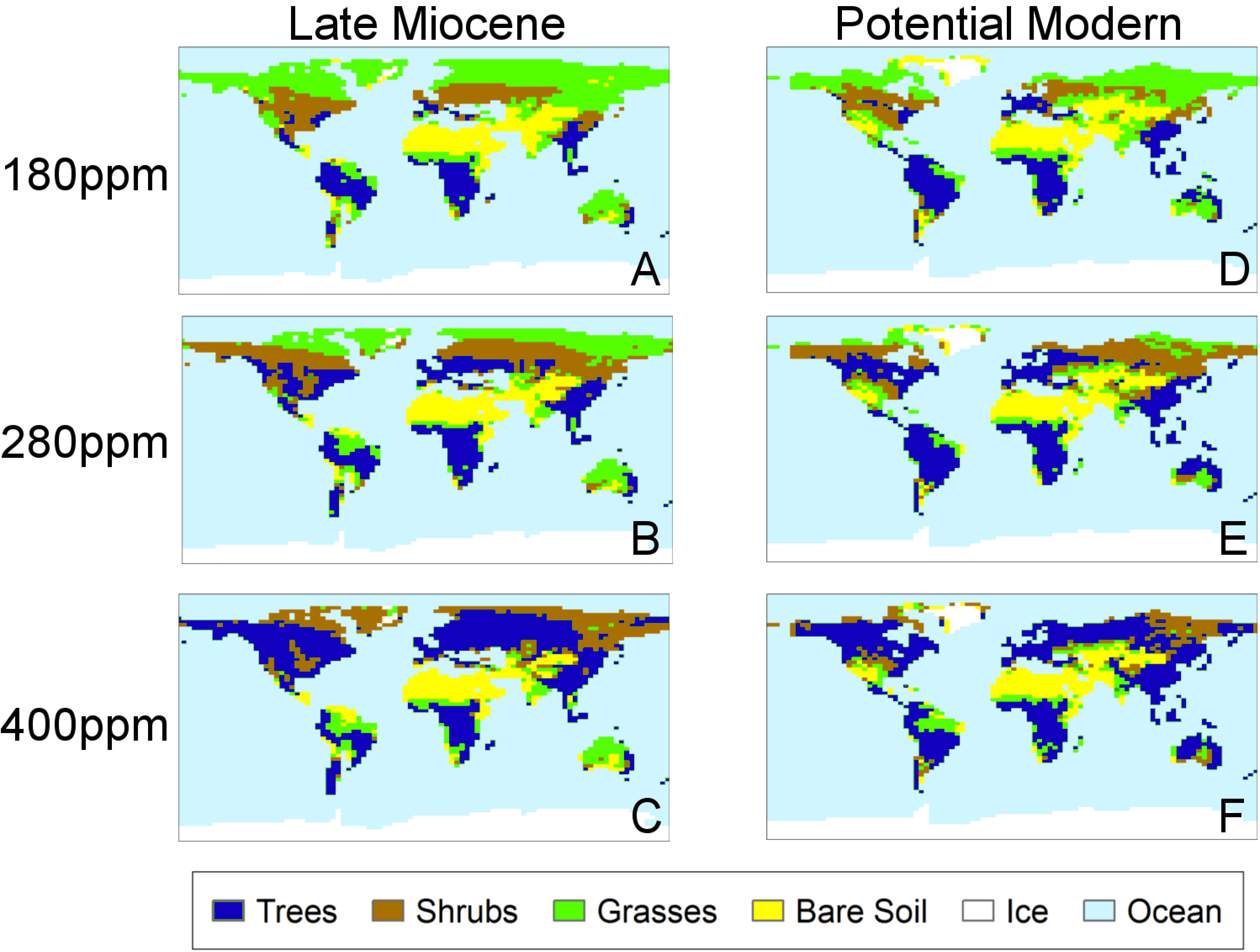

Late Miocene
Potential Modern
180ppm
280ppm
400ppm
A
B
C
D
E
F
Trees
Shrubs
Grasses
Bare Soil
Ice
Ocean

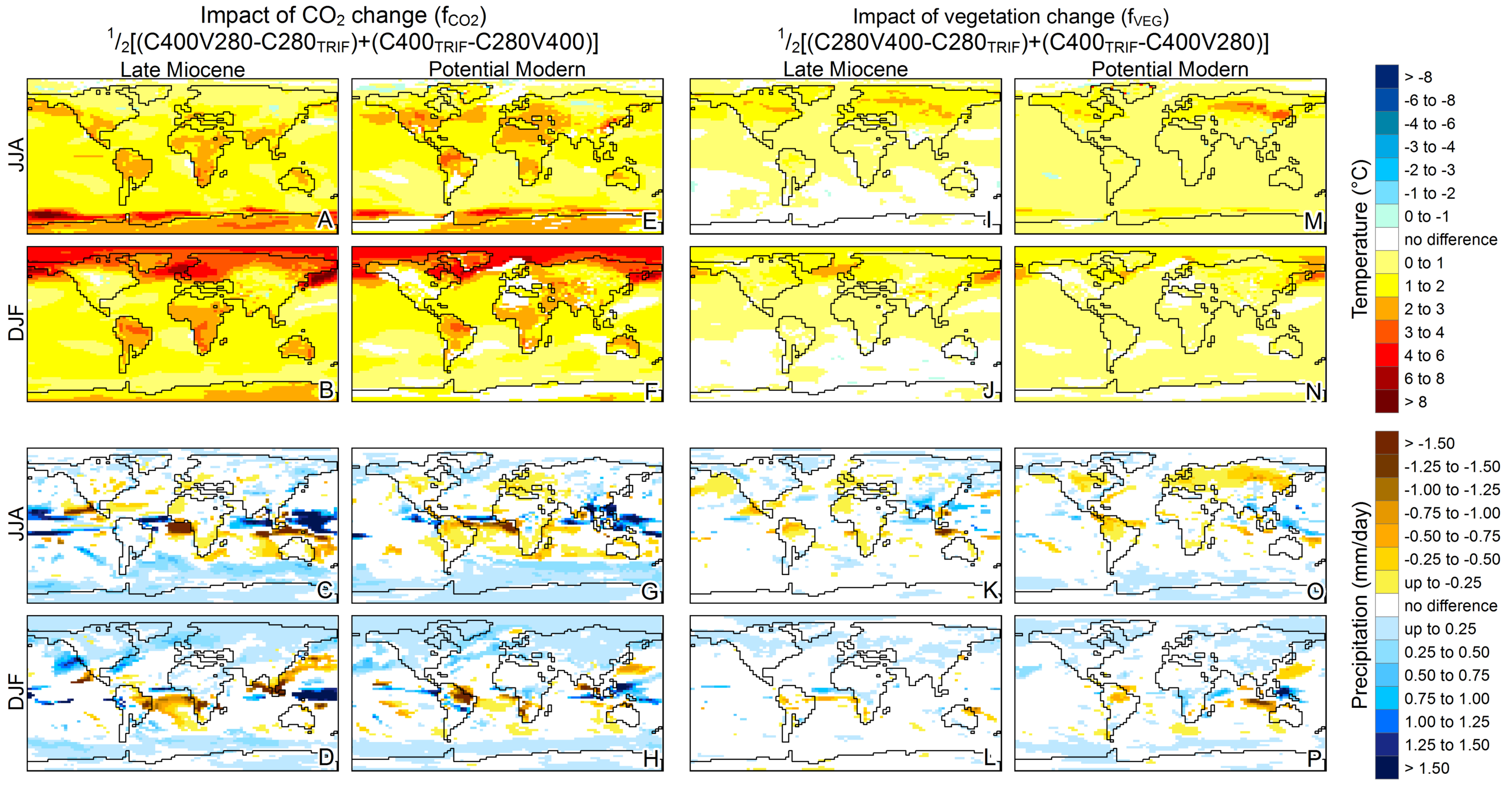
Impact of CO_2 change (f_{CO2})
$^1/_2[(C400V280-C280_{TRIF})+(C400_{TRIF}-C280V400)]$
Impact of vegetation change (f_{VEG})
$^1/_2[(C280V400-C280_{TRIF})+(C400_{TRIF}-C400V280)]$
Late Miocene
Potential Modern
Late Miocene
Potential Modern
JJA
DJF
JJA
DJF
A
B
C
D
E
F
G
H
I
J
K
L
M
N
O
P
Temperature (°C)
> -8
-6 to -8
-4 to -6
-3 to -4
-2 to -3
-1 to -2
0 to -1
no difference
0 to 1
1 to 2
2 to 3
3 to 4
4 to 6
6 to 8
> 8
Precipitation (mm/day)
> -1.50
-1.25 to -1.50
-1.00 to -1.25
-0.75 to -1.00
-0.50 to -0.75
-0.25 to -0.50
up to -0.25
no difference
up to 0.25
0.25 to 0.50
0.50 to 0.75
0.75 to 1.00
1.00 to 1.25
1.25 to 1.50
> 1.50

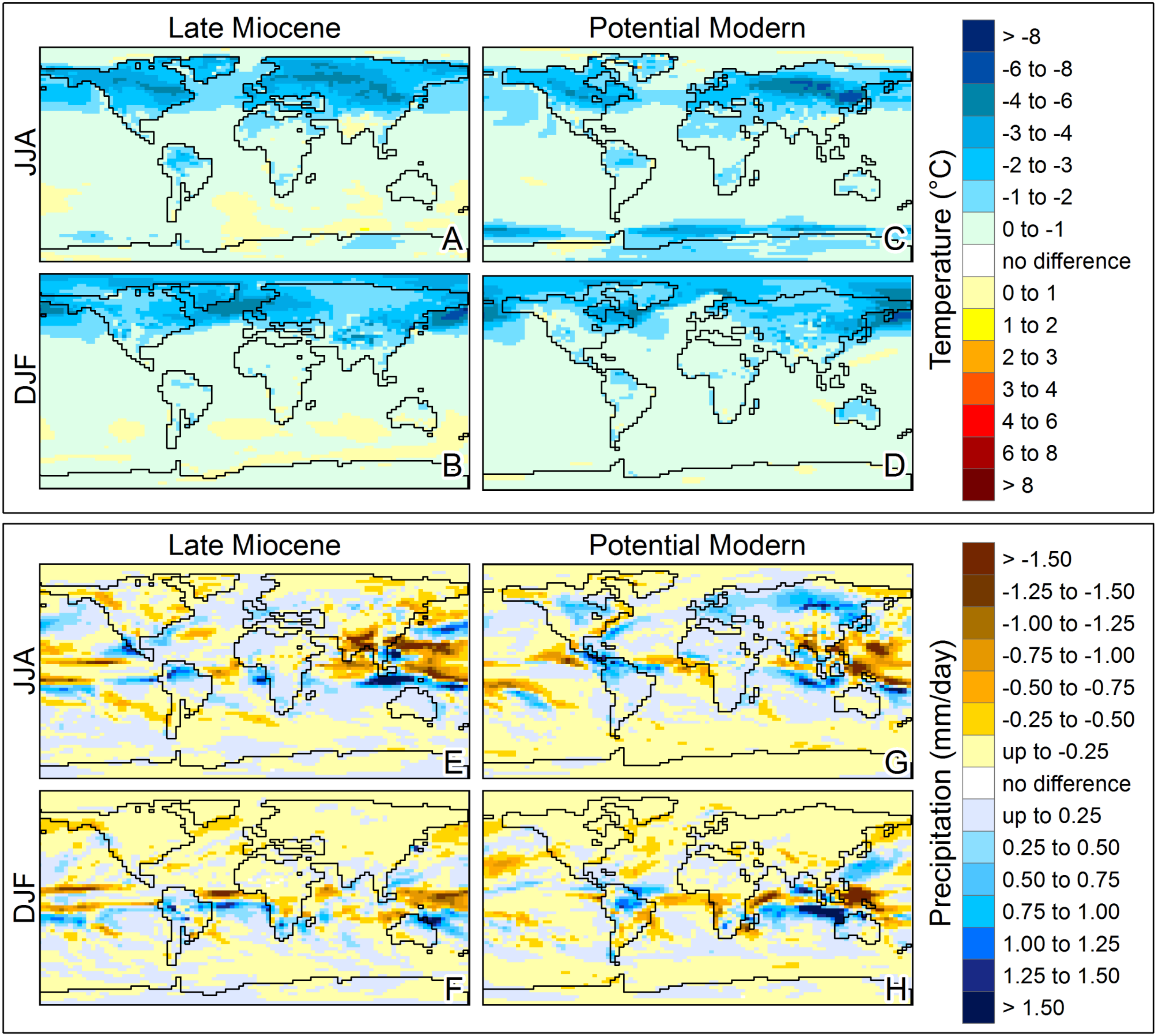

Late Miocene
Potential Modern
JJA
DJF
A
B
C
D
Temperature (°C)
> -8
-6 to -8
-4 to -6
-3 to -4
-2 to -3
-1 to -2
0 to -1
no difference
0 to 1
1 to 2
2 to 3
3 to 4
4 to 6
6 to 8
> 8
Late Miocene
Potential Modern
JJA
DJF
E
F
G
H
Precipitation (mm/day)
> -1.50
-1.25 to -1.50
-1.00 to -1.25
-0.75 to -1.00
-0.50 to -0.75
-0.25 to -0.50
up to -0.25
no difference
up to 0.25
0.25 to 0.50
0.50 to 0.75
0.75 to 1.00
1.00 to 1.25
1.25 to 1.50
> 1.50

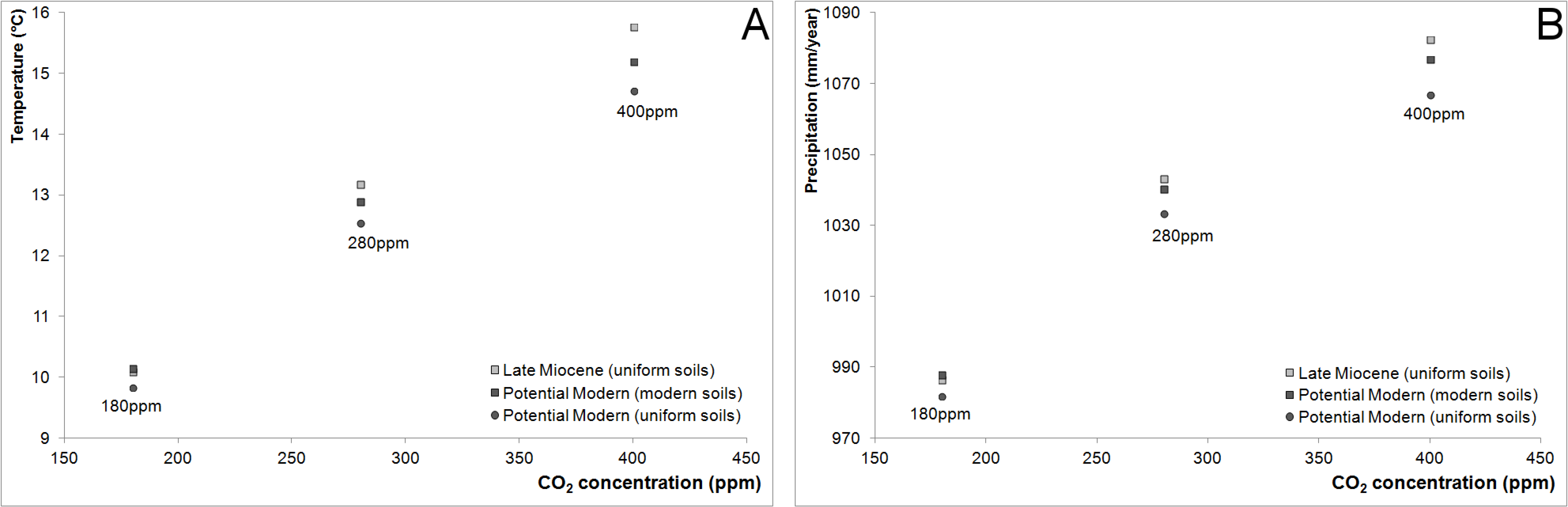

A
Temperature (°C)
16
15
14
13
12
11
10
9
400ppm
280ppm
180ppm
Late Miocene (uniform soils)
Potential Modern (modern soils)
Potential Modern (uniform soils)
150
200
250
300
350
400
450
CO_2 concentration (ppm)
B
Precipitation (mm/year)
1090
1070
1050
1030
1010
990
970
400ppm
280ppm
180ppm
Late Miocene (uniform soils)
Potential Modern (modern soils)
Potential Modern (uniform soils)
150
200
250
300
350
400
450
CO_2 concentration (ppm)

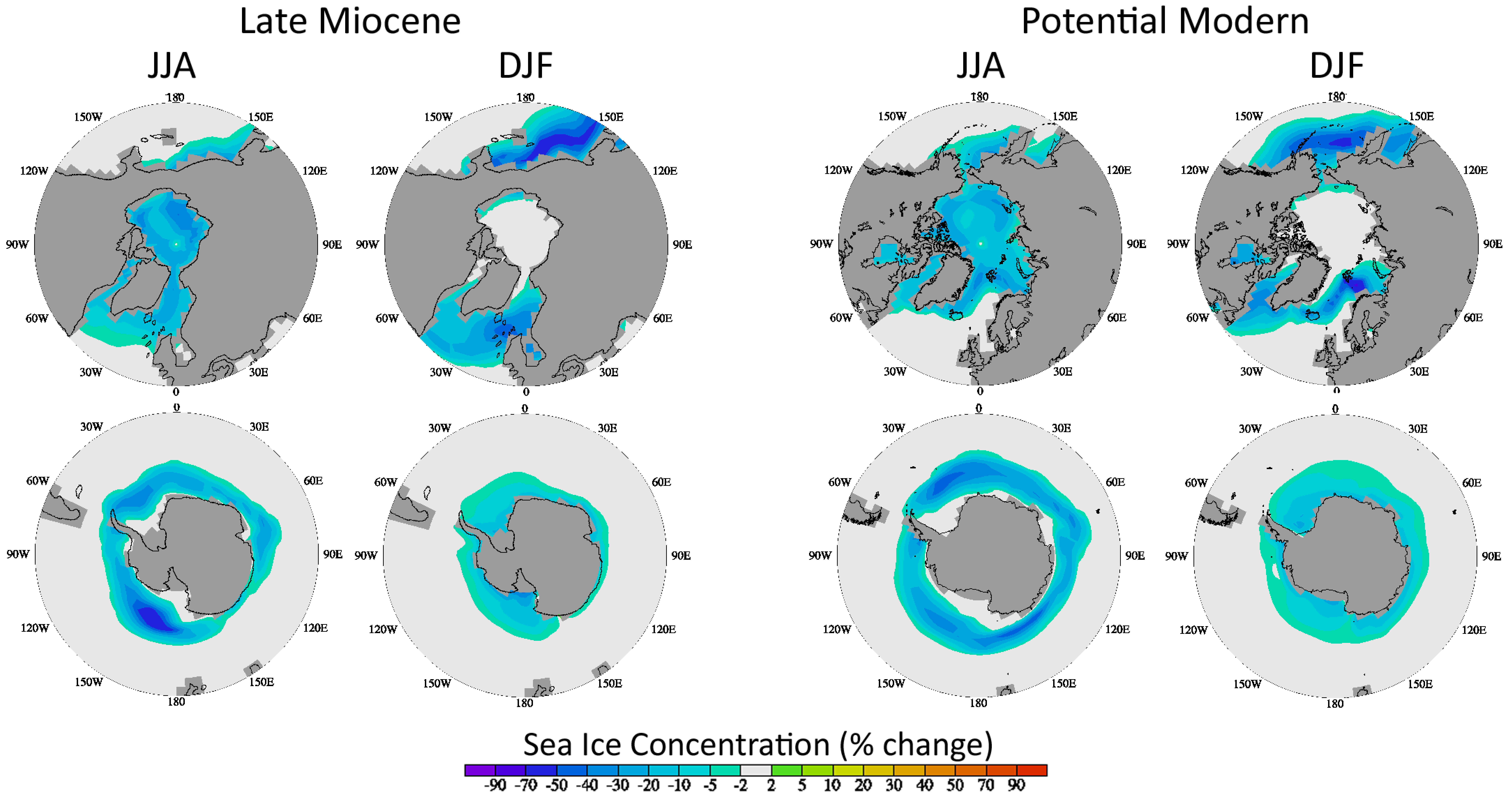
Late Miocene
Potential Modern
JJA
DJF
JJA
DJF
180
150W
150E
120W
120E
90W
90E
60W
60E
30W
30E
0
Sea Ice Concentration (% change)
-90 -70 -50 -40 -30 -20 -10 -5 -2 2 5 10 20 30 40 50 70 90

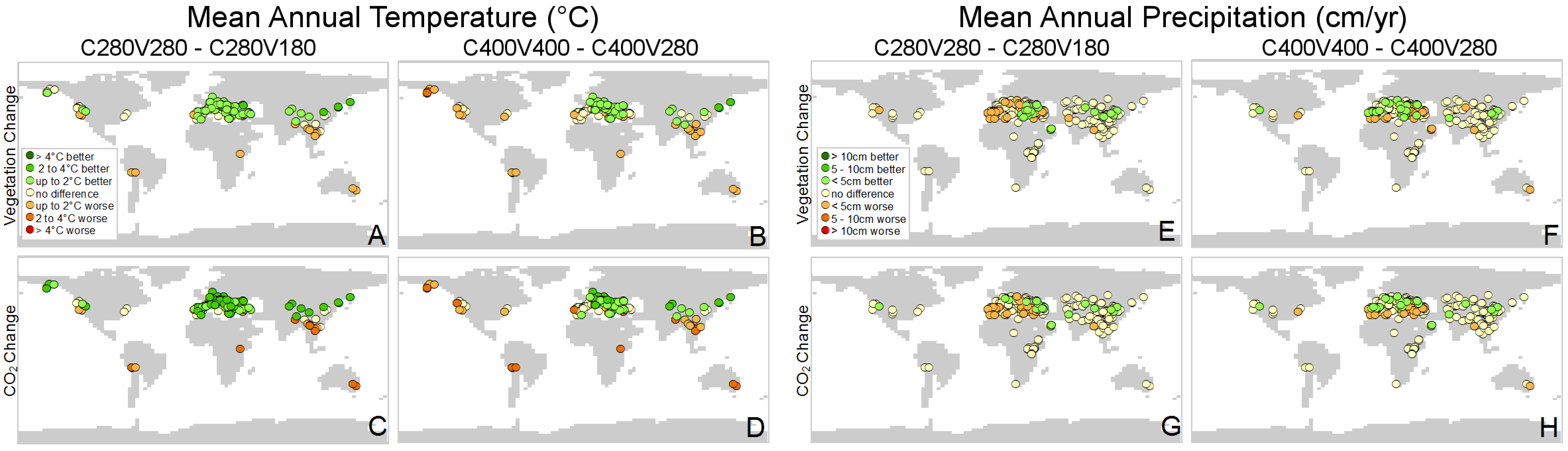

Mean Annual Temperature (°C)
Mean Annual Precipitation (cm/yr)
C280V280 - C280V180
C400V400 - C400V280
C280V280 - C280V180
C400V400 - C400V280
Vegetation Change
CO2 Change
> 4°C better
2 to 4°C better
up to 2°C better
no difference
up to 2°C worse
2 to 4°C worse
> 4°C worse
> 10cm better
5 - 10cm better
< 5cm better
no difference
< 5cm worse
5 - 10cm worse
> 10cm worse
A
B
C
D
E
F
G
H

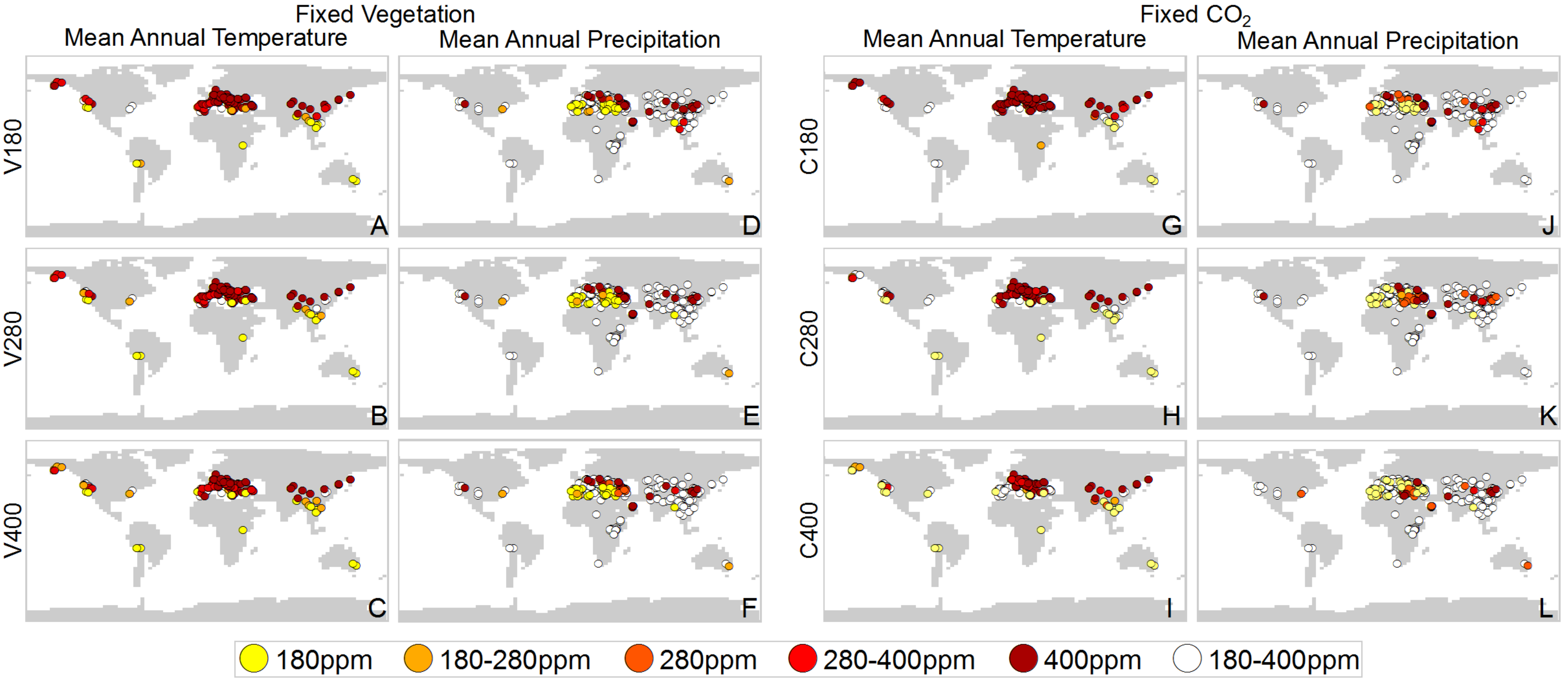

Fixed Vegetation
Mean Annual Temperature
Mean Annual Precipitation
Fixed CO_2
Mean Annual Temperature
Mean Annual Precipitation
V180
V280
V400
C180
C280
C400
A
B
C
D
E
F
G
H
I
J
K
L
180ppm
180-280ppm
280ppm
280-400ppm
400ppm
180-400ppm